J Neurophysiol 123: 1849–1863, 2020.
First published April 8, 2020; doi:10.1152/jn.00577.2019.

RESEARCH ARTICLE | *Cellular and Molecular Properties of Neurons*

Heterogeneity of neuronal firing type and morphology in retrosplenial cortex of male F344 rats

Hanna Yousuf,[1]* Andrew N. Nye,[1]* and James R. Moyer, Jr.[1,2]
[1]*Department of Psychology, University of Wisconsin-Milwaukee, Milwaukee, Wisconsin; and* [2]*Department of Biological Sciences University of Wisconsin-Milwaukee, Milwaukee, Wisconsin*

Submitted 6 September 2019; accepted in final form 7 April 2020

Yousuf H, Nye AN, Moyer JR Jr. Heterogeneity of neuronal firing type and morphology in retrosplenial cortex of male F344 rats. *J Neurophysiol* 123: 1849–1863, 2020. First published April 8, 2020; doi:10.1152/jn.00577.2019.—The rodent granular retrosplenial cortex (gRSC) has reciprocal connections to the hippocampus to support fear memories. Although activity-dependent plasticity occurs within the RSC during memory formation, the intrinsic and morphological properties of RSC neurons are poorly understood. The present study used whole-cell recordings to examine intrinsic neuronal firing and morphology of neurons in layer 2/3 (L2/3) and layer 5 (L5) of the gRSC in adult male rats. Five different classifications were observed: regular-spiking (RS), regular-spiking afterdepolarization (RS_{ADP}), late-spiking (LS), burst-spiking (BS), and fast-spiking (FS) neurons. RS_{ADP} neurons were the most commonly observed neuronal class, identified by their robust spike frequency adaptation and pronounced afterdepolarization (ADP) following an action potential (AP). They also had the most extensive dendritic branching compared with other cell types. LS neurons were predominantly found in L2/3 and exhibited a long delay before onset of their initial AP. They also had reduced dendritic branching compared with other cell types. BS neurons were limited to L5 and generated an initial burst of two or more APs. FS neurons demonstrated sustained firing and little frequency adaptation and were the only nonpyramidal firing type. Relative to adults, RS neurons from juvenile rats (PND 14–30) lacked an ADP and were less excitable. Bath application of group 1 mGluR blockers attenuated the ADP in adult neurons. In other fear-related brain structures, the ADP has been shown to enhance excitability and synaptic plasticity. Thus, understanding cellular mechanisms of the gRSC will provide insight regarding its precise role in memory-related processes across the lifespan.

NEW & NOTEWORTHY This is the first study to demonstrate that granular retrosplenial cortical (gRSC) neurons exhibit five distinctive firing types: regular spiking (RS), regular spiking with an afterdepolarization (RS_{ADP}), late spiking (LS), burst spiking (BS), and fast spiking (FS). RS_{ADP} neurons were the most frequently observed cell type in adult gRSC neurons. Interestingly, RS neurons without an ADP were most common in gRSC neurons of juvenile rats (PND 14–30). Thus, the ADP property, which was previously shown to enhance neuronal excitability, emerges during development.

afterdepolarization; brain slice electrophysiology; intrinsic excitability; late spiking; layer 2/3; layer 5

INTRODUCTION

The rodent retrosplenial cortex (RSC) is a brain structure critical for processing spatial and associative fear memories (Corcoran et al. 2011; Keene and Bucci 2008a, 2008b, 2008c, 2009; Kwapis et al. 2015; Miller et al. 2014; Robinson et al. 2012; Todd and Bucci 2015). Memory-associated immediate early gene (IEG; e.g., c-fos, arc, zif268) expression in the RSC is elevated following spatial and contextual fear learning (Maviel et al. 2004; Robinson et al. 2012; Cowansage et al. 2014; Tanaka et al. 2014). The RSC may support memory formation through its dense reciprocal connections with the thalamus and hippocampus (Coelho et al. 2018; Corcoran et al. 2016; Robinson et al. 2018; van Groen et al. 1993, 2004; Yamawaki et al. 2019). For example, hippocampal lesions reduced IEG expression in the RSC (Albasser et al. 2007). In addition to activity-dependent changes in gene expression in the RSC, synaptic plasticity occurs in the form of long-term potentiation (LTP) or long-term depression (LTD), which are fundamental mechanisms underlying memory formation (Martin and Morris 2002). Lesions to the anterior thalamus result in a loss of LTD (Garden et al. 2009) and neuronal excitability (Gabriel et al. 1983) in the RSC. Despite the growing knowledge that the RSC undergoes activity-dependent plastic changes, which are required for memory processing, the physiology of this region remains poorly understood.

The RSC has two distinct subregions, granular (area 29) and dysgranular (area 30), that may be morphologically and functionally distinct (van Groen et al. 1993, 2004; van Groen and Wyss 1990). Because of its extensive connections with the thalamus and hippocampus, the majority of behavioral and electrophysiological studies have targeted the granular RSC (gRSC; Chen et al. 1994; Cho and Sharp 2001; Corcoran et al. 2011; Garden et al. 2009; Kwapis et al. 2015; Pothuizen et al. 2009; van Groen et al. 2004). To date, studies have only reported intrinsic properties of the gRSC using juvenile rats between postnatal days (PND) 20 and 35, and those studies reported the existence of regular-spiking (RS) and late-spiking (LS) neurons (Brennan et al. 2020; Kurotani et al. 2013). Previous work has demonstrated that neuronal physiology in other fear-related brain structures, including the amygdala and hippocampus, go through drastic changes before adulthood (Ehrlich et al. 2012; Vasilyev and Barish 2002). Therefore, the present study takes a step forward and demonstrates that the traditional RS neuron, prevalent in the juvenile gRSC, is rarely

* H. Yousuf and A. N. Nye contributed equally to this article.
Correspondence: J. R. Moyer, Jr. (e-mail: jrmoyer@uwm.edu).

observed in the adult gRSC. Moreover, this is the first study to elucidate the existence of five distinct firing patterns in the adult gRSC, which include regular-spiking (RS), regular-spiking afterdepolarization (RS_{ADP}), late-spiking (LS), burst-spiking (BS), and fast-spiking (FS) neurons. The most abundant firing type is the RS_{ADP} neuron that has a prominent afterdepolarization (ADP) following a single action potential (AP). Interestingly, this pronounced ADP is absent in juvenile rats (e.g., PND 14–30). In neuronal subpopulations of the hippocampus, the ADP following a single AP has been shown to be mediated by the activation of metabotropic glutamate receptors (mGluRs; Young et al. 2004). We further established that the ADP property in adult gRSC neurons is also partially mediated by mGluRs. Given the important role that the RSC plays in learning and memory, understanding the intrinsic and morphological properties may elucidate the precise mechanisms through which the gRSC contributes to the consolidation or retrieval of spatial and fear memories.

METHODS

Subjects

Subjects were adult (PND ~90) and juvenile (PND 14–30) F344 male rats. Rats were maintained in an AAALAC (Association for Assessment and Accreditation of Laboratory Animal Care) accredited facility on a 14:10-h light-dark cycle and housed individually with ad libitum access to food and water. Procedures were conducted in accordance with National Institutes of Health guidelines and approved by the University of Wisconsin-Milwaukee Animal Care and Use Committee.

RSC Slice Preparation

Rats were deeply anesthetized with isoflurane, and an intracardiac perfusion was performed with ice-cold, oxygenated, sucrose-artificial cerebrospinal fluid (aCSF; composition in mM: 206 sucrose, 26 $NaHCO_3$, 10 D-glucose, 2.80 KCl, 2 $MgSO_4 \cdot 7H_2O$, 1.25 $NaH_2PO_4 \cdot H_2O$, 1 $CaCl_2$, 1 $MgCl_2$, and 0.40 Na-ascorbate). Brains were rapidly removed and placed in ice-cold oxygenated sucrose-aCSF and blocked with three dissections (anterior and posterior sections, and a portion of left hemisphere was removed). Coronal brain slices (400 μm) containing the RSC (anteroposterior from −1.80 to −3.80 mm) were cut in oxygenated sucrose-aCSF at ~1°C using a vibrating tissue slicer (VT1200; Leica). Slices were then transferred to a holding chamber (Moyer and Brown 1998) containing oxygenated aCSF (composition in mM: 124 NaCl, 26 $NaHCO_3$, 20 D-glucose, 2.80 KCl, 2 $MgSO_4 \cdot 7H_2O$, 1.25 $NaH_2PO_4 \cdot H_2O$, and 2 $CaCl_2$) at 32–36°C and allowed to recover for ~30 min. Brain slices were then placed at room temperature and allowed to recover for another 30 min before recordings.

Electrophysiological Recordings

An Olympus BX51WI upright microscope outfitted with a submerged recording chamber and equipped with infrared DIC optics was used for visualizing the neuron and patch electrode. Slices were transferred to the chamber, where they were perfused at a rate of 2.1 mL/min (maintained at 32–36°C using an inline temperature controller). Whole-cell recordings were made from L2/3, and L5 (Fig. 1) of the anterior gRSC (anteroposterior approximately −1.80 to −3.80). For whole-cell recordings, electrodes (~4–5 MΩ) were prepared from thin-walled capillary glass and filled with the following solution (in mM): 110 K-gluconate, 20 KCl, 10 Di-Tris-P-creatine, 10 HEPES, 2 $MgCl_2$, 2 Na_2ATP, 0.3 Na_2GTP, and 0.2% biocytin, pH to 7.3. All recordings were obtained in current clamp mode (holding potential −67.0 ± 3 mV) using a HEKA EPC10 amplifier system (HEKA instruments Inc., Bellmore, NY). Series resistance was fully compensated and consistently monitored to ensure the stability of recording conditions, and cells were analyzed only if the initial series resistance did not change by >30% throughout the recording period. Experiments were controlled by PatchMaster software (HEKA Instruments) running on a PC, and data were transferred to a PC using an ITC-16 digital-to-analog converter (HEKA Instruments). The signals were filtered at 2.9 kHz and digitized at 20 kHz using PatchMaster software. Data were analyzed using PatchMaster and Igor Pro software (version 6.37; Wavemetrics).

Intrinsic properties of gRSC neurons were studied in current clamp conditions using the following protocols (Song et al. 2015; Song and Moyer 2018). *1*) *V-I* relationships were obtained from a series of 0.5-s current injections (ranging from −300 to +50 pA), and the plateau voltage deflection was plotted against the current amplitude. Neuronal input resistance (R_N) was determined from the slope of the linear fit of the portion of the *V–I* plot, where the voltage sweeps were symmetrical. Similarly, the membrane time constant (τ) was defined as 63%

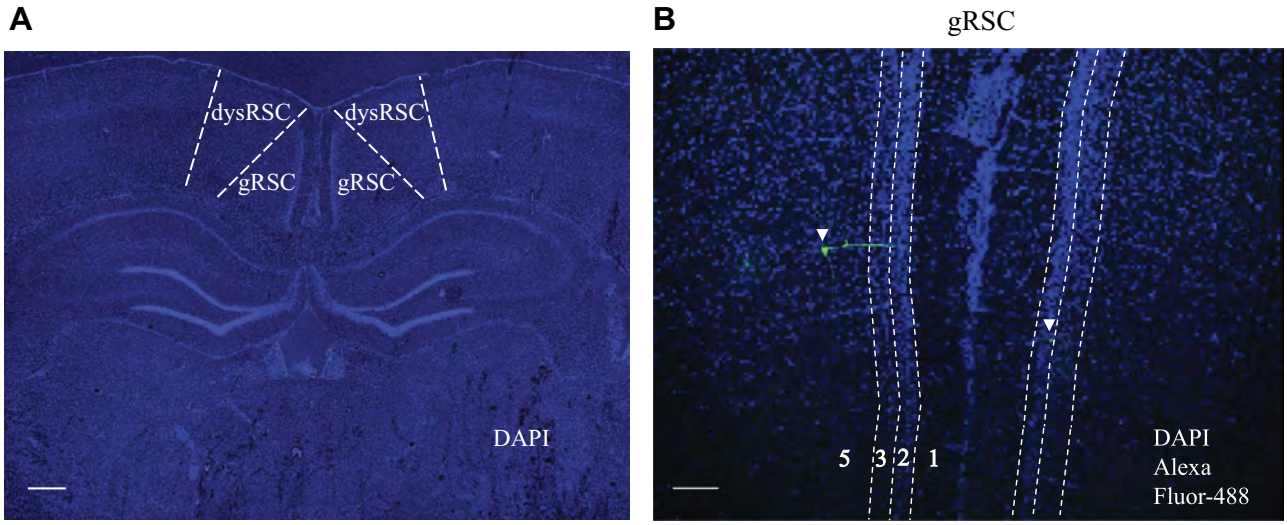

Fig. 1. Fluorescence images showing coronal sections of rat retrosplenial cortex (RSC). *A*: low-power (×4) DAPI image illustrating the borders of granular RSC (gRSC) and dysgranular RSC (dysRSC; scale bar, 500 μm). *B*: representative dual-channel DAPI and Alexa flour-488 images (×10) used to determine the laminar location of recorded neurons. *Left* arrowhead, a L5 neuron; *right* arrowhead, a layer 3 neuron (scale bar, 50 μm).

of the time until plateau voltage deflection and the average τ for each neuron were calculated from the symmetrical voltage sweeps (e.g, those that did not exhibit sags or active conductance). The sag ratio during hyperpolarizing membrane responses was expressed as $[(1 - \Delta V_{ss}/\Delta V_{max}) \times 100\%]$, where $\Delta V_{ss} = MP - V_{ss}$ and $\Delta V_{max} = MP - V_{max}$ (MP is the membrane potential before the current step, V_{ss} is the steady-state potential at the end of the current step, and V_{max} is the peak amplitude during the first 150 ms of the current step). For each neuron, the sag ratio was calculated from −300, −250, and −200 pA current injections and averaged. *2*) AP properties were studied with an ascending series of 0.5- or 1-s depolarizing pulses (5-pA increments). At rheobase, neurons could be classified as RS_{ADP} (Fig. 2*A*), LS (Fig. 3*A*), BS (Fig. 4*A*), or FS (Fig. 5*A*). Cells were classified by firing type based on how the cell responded to suprathreshold current injections.

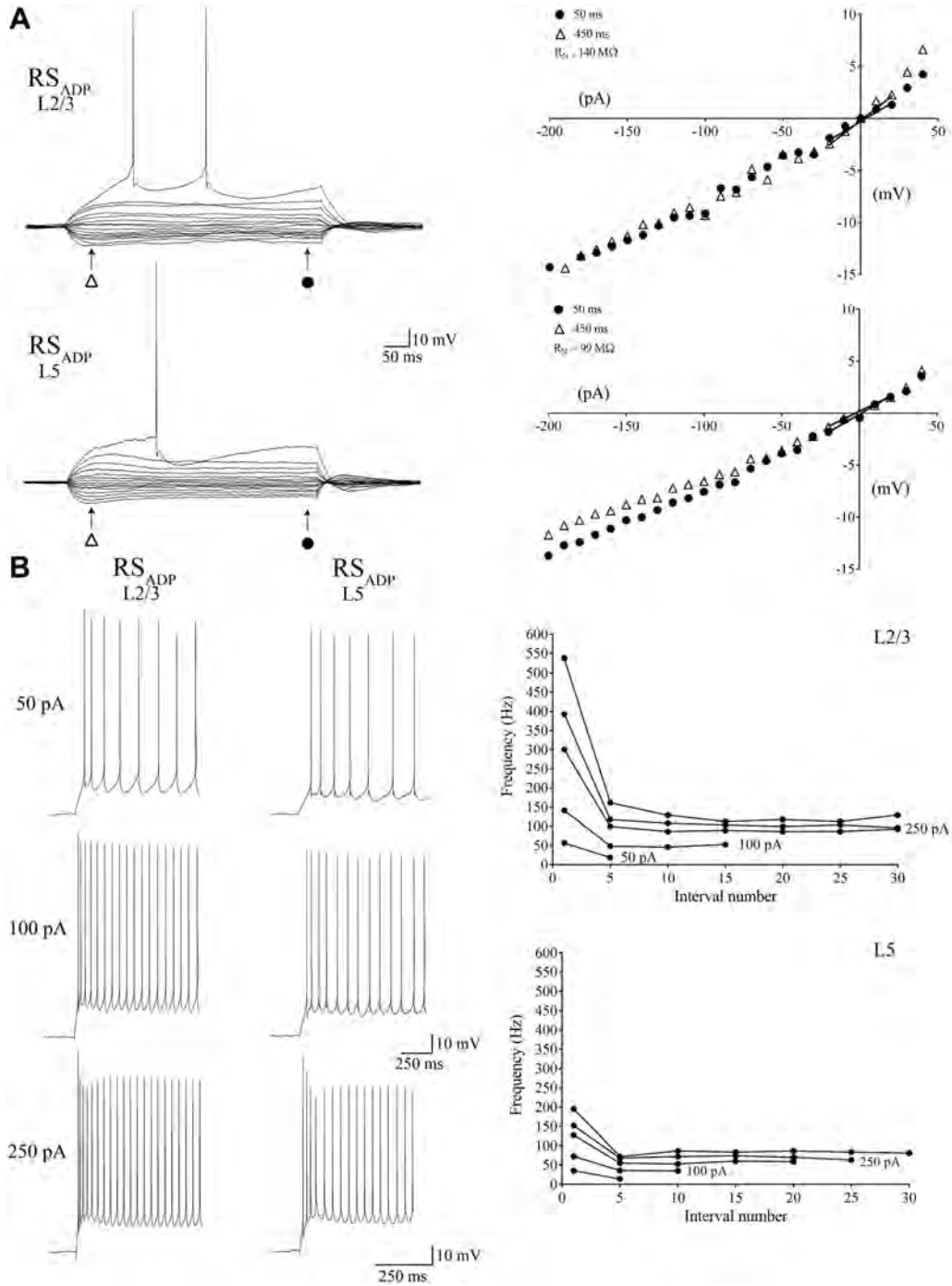

Fig. 2. Intrinsic properties of L2/3 and L5 regular-spiking afterdepolarization (RS_{ADP}), neurons. *A*, *left*: representative waveforms of RS_{ADP} neuron in response to hyperpolarizing and depolarizing current injections. RS_{ADP} neurons show pronounced depolarizing and hyperpolarizing sags. In response to suprathreshold current injections, RS_{ADP} neurons usually fire an action potential early during the current step. *A*, *right*: voltage-current (*V-I*) relation of RS_{ADP} neurons from L2/3 (R_N = 140 MΩ) and L5 (R_N = 99 MΩ). ●, Measurements taken at 50 ms after onset of current pulse; △, measurements taken at 450 ms after onset of current pulse. *B*, *left*: representative waveforms of RS_{ADP} neurons in L2/3 and L5 in response to a series of 1-s, suprathreshold depolarizing current injections. *B*, *right*: plots of the firing frequency vs. interval number from the L2/3 (*top*) and L5 (*bottom*) RS_{ADP} neurons. Both frequency plots have a downward curve, indicating that RS_{ADP} neurons in both layers are adapting.

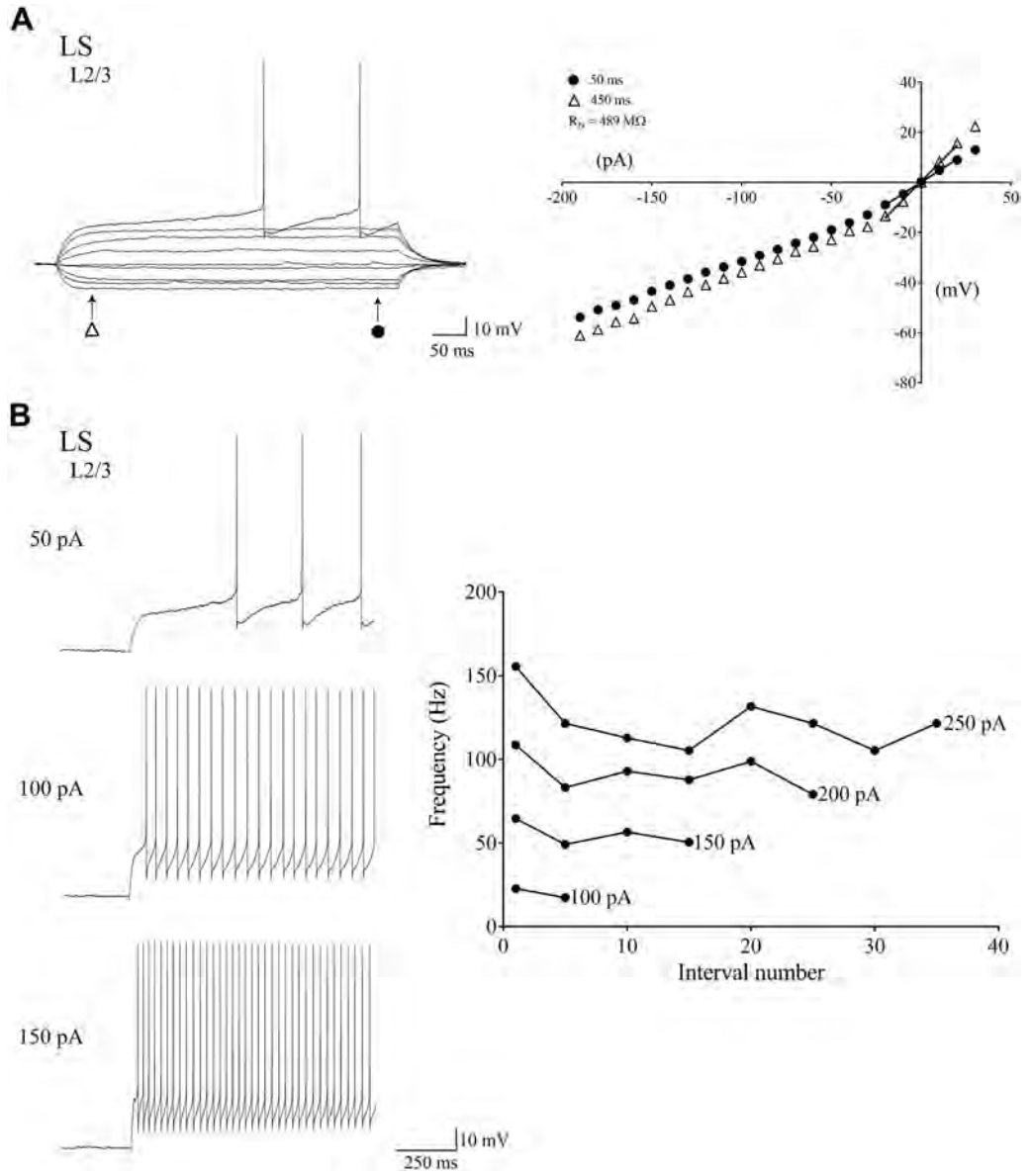

Fig. 3. Intrinsic properties of L2/3 late-spiking (LS) neurons. *A*, *left*: representative voltage responses of a LS neuron in response to hyperpolarizing and depolarizing current injections. Note that LS neurons show minimal voltage sag. In response to just-suprathreshold current injections, LS neurons fire action potentials near the end of the current step. ●, Measurements taken at 50 ms after onset of current pulse; △, measurements taken at 450 ms after onset of current pulse. *A*, *right*: voltage-current (*V-I*) relation of L2/3 LS neuron (R_N = 489 MΩ). *B*, *left*: representative voltage responses of an LS neuron in response to a series of 1-s suprathreshold depolarizing current injections. *B*, *right*, a plot of firing frequency vs. interval number. Frequency plot is fairly flat and linear, indicating that LS neurons show only mild spike frequency adaptation.

RS_{ADP} neurons were defined as neurons that fired a single AP at rheobase within ~350 ms of onset of a 500-ms current injection. The ADP was identified as the depolarizing crest between the fast afterhyperpolarization (fAHP) and the point at which membrane voltage returned to resting potential (Metz et al. 2005; Storm 1987; Yue and Yaari 2004). This depolarization crest following a fAHP was completely absent in RS neurons of the juvenile gRSC. LS neurons were defined as neurons that exhibited delayed firing of an AP until the end of the current injection (~700 ms in a 1-s current injection; Faulkner and Brown 1999; Kurotani et al. 2013; Moyer et al. 2002). BS neurons were defined as neurons that fire two or more APs in short succession (~8 ms) at rheobase. FS neurons were defined as neurons that displayed no repetitive burst firing, fired short duration APs (e.g., half width < 0.5 ms; see Faulkner and Brown 1999), and had rapid, sharp afterhyperpolarizations (AHPs; see Brennan et al. 2020). For all neurons, AP properties were studied from the first AP. Current threshold ($I_{threshold}$) was defined as the minimum amount of depolarizing current required to evoke an AP from a recorded neuron. $AP_{threshold}$ was defined as the membrane voltage at which d*V*/d*t* first exceeded 28 mV/ms (Kaczorowski et al. 2012). $AP_{latency}$ was defined as the time to the peak of the first AP relative to the onset of the current injection. $AP_{amplitude}$ was measured relative to the $AP_{threshold}$, and fAHP was also measured relative to $AP_{threshold}$. $ADP_{amplitude}$ was measured relative to fAHP. For drug experiments, an average $ADP_{amplitude}$ was calculated pre- and post-drug application by measuring $ADP_{amplitude}$ at rheobase and from the first AP in subsequent current injections close to rheobase (within 20 pA). Finally, $AP_{half\text{-}width}$ was measured as the width at half of the $AP_{amplitude}$. *3*) Post-burst AHP was studied after a 50-Hz burst of 10 spikes, each of which was evoked by a 2-ms suprathreshold current injection (3 times at 20-s intervals). After the last AP, the post-burst AHP was measured at the peak amplitude. Slow afterhyperpolarization (sAHP) was measured 1 s following

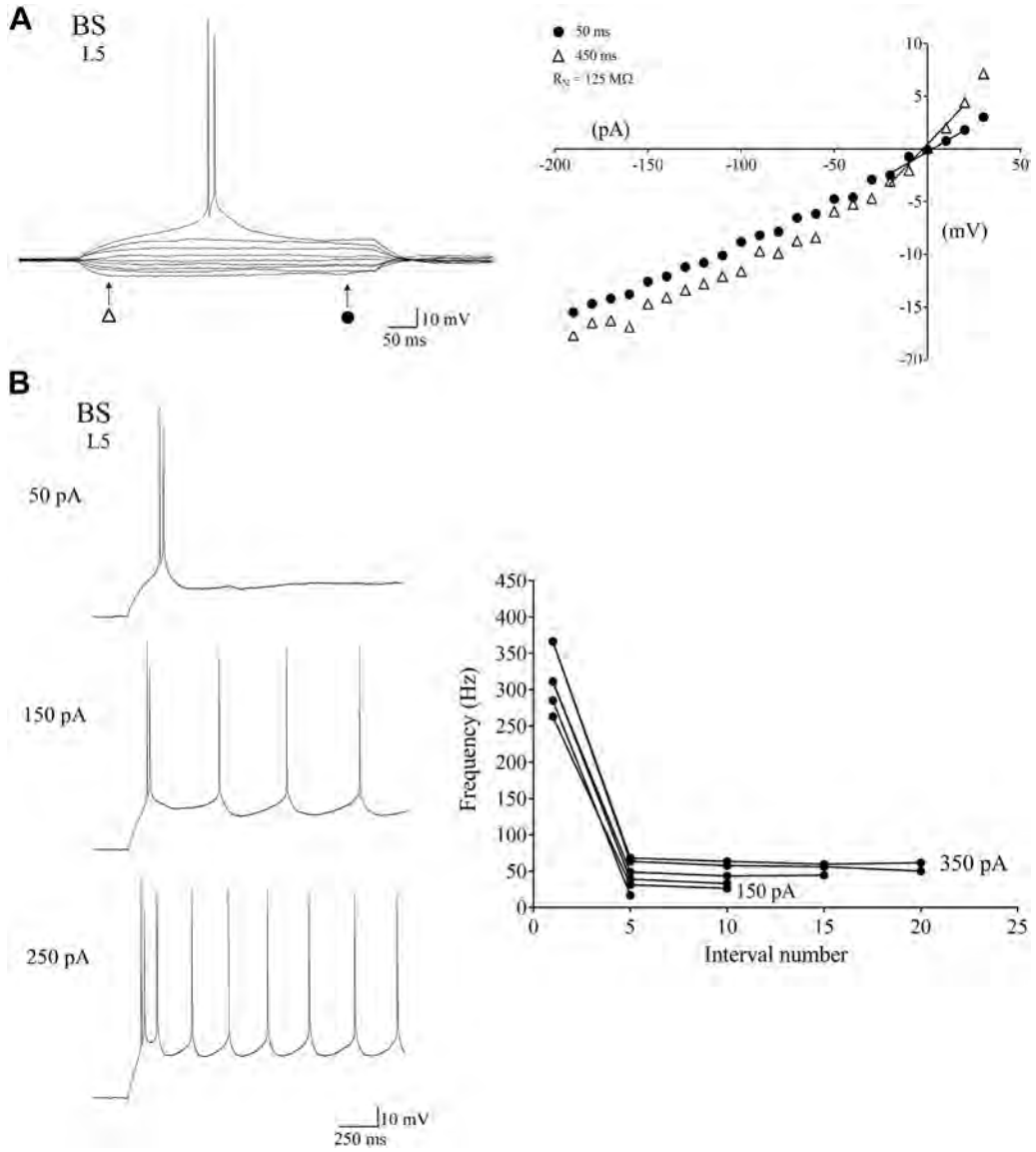

Fig. 4. Intrinsic properties of L5 burst-spiking (BS) neurons. *A*, *left*: representative waveforms of a BS neuron in response to hyperpolarizing and depolarizing current injections. BS neurons show minimal voltage sags. In response to suprathreshold current injections, BS neurons usually fire action potentials early during the current step. *A*, *right*: voltage-current (*V-I*) relation of an L5 BS neuron (R_N = 125 MΩ). ●, Measurements taken at 50 ms after onset of current pulse; △, measurements taken at 450 ms after onset of current pulse. *B*, *left*: representative voltage responses of BS neurons in response to a series of 1-s suprathreshold depolarizing current injections. B, *right*: a plot of firing frequency vs. interval number. Note the rapid downward curve of the frequency plots, indicating that BS neurons exhibit spike frequency adaptation.

the offset of current injection. *4*) Neuronal excitability was assessed by counting the number of spikes evoked in response to a series of 5-s depolarizing steps (range was from 0 to 450 pA in 25-pA increments). Initial firing frequency was calculated from the interspike interval (ISI) of the first two APs.

Pharmacological Agents

The following pharmacological agents were used in the experiments: (S)-(+)-α-amino-4-carbody-2-methylbenzeneacetic acid [LY367385 (mGluR1 antagonist), 10 μM, 100 μM] and 2-methyl-6-(phenylethynyl) pyridine hydrochloride [MPEP (mGluR5 antagonist), 10 μM, 100 μM], all obtained from Tocris (Bio-Techne, Minneapolis, MN).

Biocytin Staining

All neurons were filled with biocytin to confirm the location and perform morphological analyses of cells in the gRSC. After completion of whole-cell recordings, slices were fixed in formalin and kept at 4°C for ≥1 day and ≤10 days before further processing. To visualize neurons labeled by biocytin, the slices were washed with 0.1 M phosphate-buffered saline (PBS) for 5 min (3 times). Slices were then incubated in H_2O_2-methanol for 45 min and then washed again with 0.1 M PBS for 5 min (3 times), followed by Triton X-100/BSA for 45 min. Then slices were incubated with 1:500 Streptavidin-Alexa Fluor-488 (Invitrogen) for 120 min in the dark or overnight at 4°C in the dark. Slices were then washed with 0.1 M PBS for 5 min (3 times) and subsequently mounted on slides, coverslipped with DAPI containing Ultra Cruz Mounting Medium (Santa Cruz Biotechonology, Houston, TX) and sealed with nail polish.

Neuron Imaging, Reconstruction, and Analysis

The neurons previously processed with Streptavidin-Alexa Fluor-488 were viewed under a fluorescence microscope at ×2 and ×100 and photographed using an Olympus BX51 upright microscope with

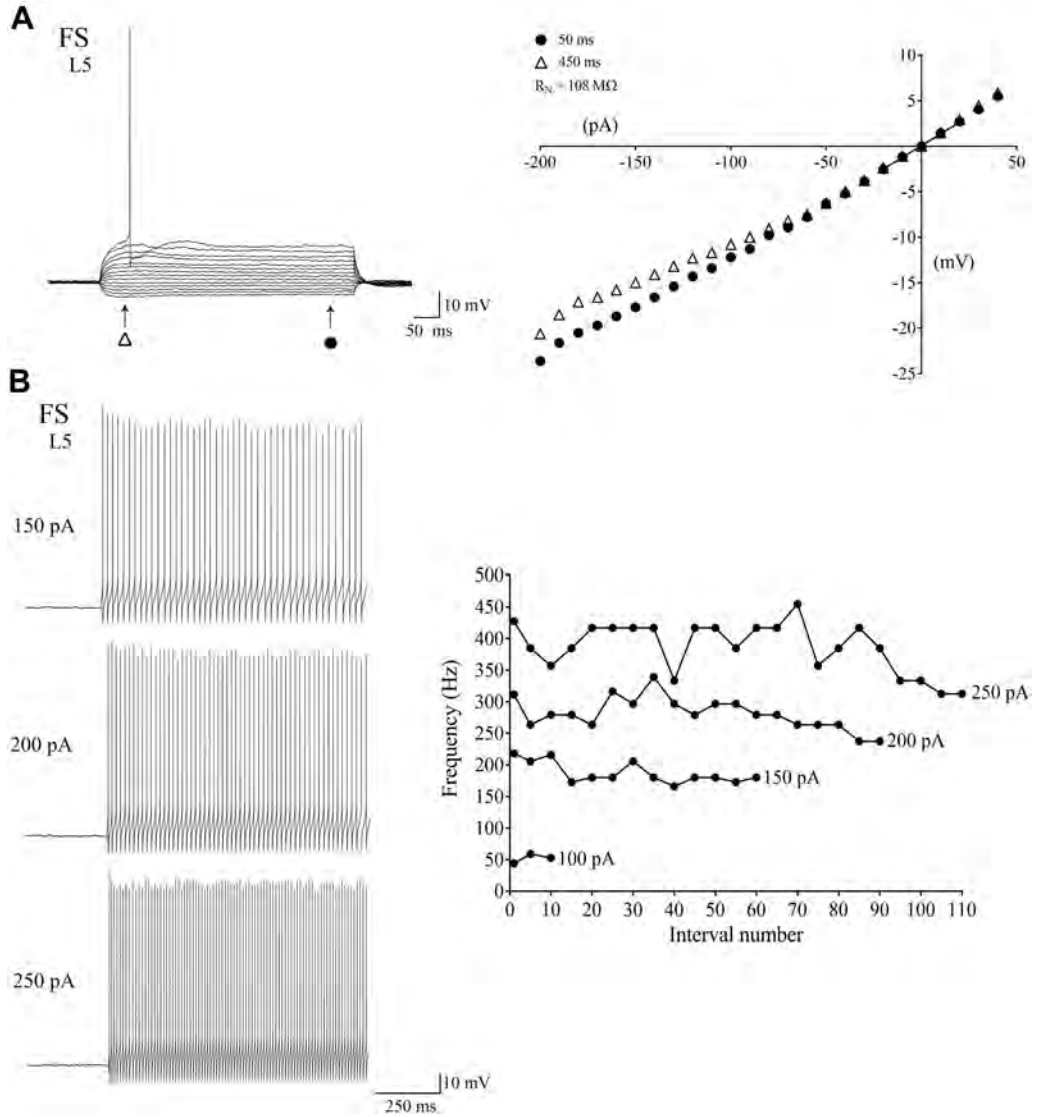

Fig. 5. Intrinsic properties of L5 fast-spiking (FS) neurons. *A*, *left*: representative waveforms of a FS neuron in response to hyperpolarizing and depolarizing current injections. FS neurons show minimal to no voltage sag. In response to suprathreshold current injections, FS neurons usually fire action potentials early during the current step. *A*, *right*: voltage-current (*V-I*) relation of L5 FS neuron (R_N = 108 MΩ). ●, Measurements taken at 50 ms after onset of current pulse; △, measurements taken at 450 ms after onset of current pulse. *B*, *left*: representative voltage responses of FS neurons in response to a series of 1-s suprathreshold depolarizing current injections. *B*, *right*: a plot of firing frequency vs. interval number. Frequency plots are linear and quite flat, indicating that FS neurons exhibit little spike frequency adaptation.

attached CCD camera (Olympus microscopy). At ×2, an image of the hippocampus was captured to determine approximate anterior/posterior location of slice. The stained neurons were also viewed under a confocal microscope (Olympus FV1000) using a ×10 objective to capture a dual channel image (DAPI and Alexa Fluor-488) for determining laminar location of neurons (Fig. 1). Confocal images were also obtained using ×20 and ×100 objectives to capture additional *Z*-stacks and create three-dimensional images of RSC neurons (Fig. 6). The ×20 image stacks were then used to reconstruct stained neurons using Neurolucida, 360 and subsequent Sholl analysis was performed with Neurolucida Explorer (MBF Bioscience, Williston, VT).

Statistical Analyses

For all whole-cell recordings and neuronal reconstructions, data were averaged based on the firing type of the cell and were reported as means ± SE. The overall differences between firing types were examined using one-way or repeated-measures ANOVA using GraphPad Prism 7.00 (GraphPad Software, Inc., La Jolla, CA). For each significant F ratio (0.05 level), post hoc Fisher least significant difference (LSD) test was used to determine specific differences between firing types. For all drug experiments, one-way ANOVA and Sidak's multiple-comparisons test were used to evaluate drug effects.

RESULTS

Physiology and Morphology of RS_{ADP} Neurons in L2/3 and L5 of the Adult gRSC

The most commonly observed firing type in the adult rat gRSC was the RS_{ADP} (61%, 71 of 116; Table 1). All RS_{ADP} neurons were identified as pyramidal at the time of recordings using DIC optics, and this was confirmed with reconstructions. The majority of RS_{ADP} neurons reside in L5 of the gRSC

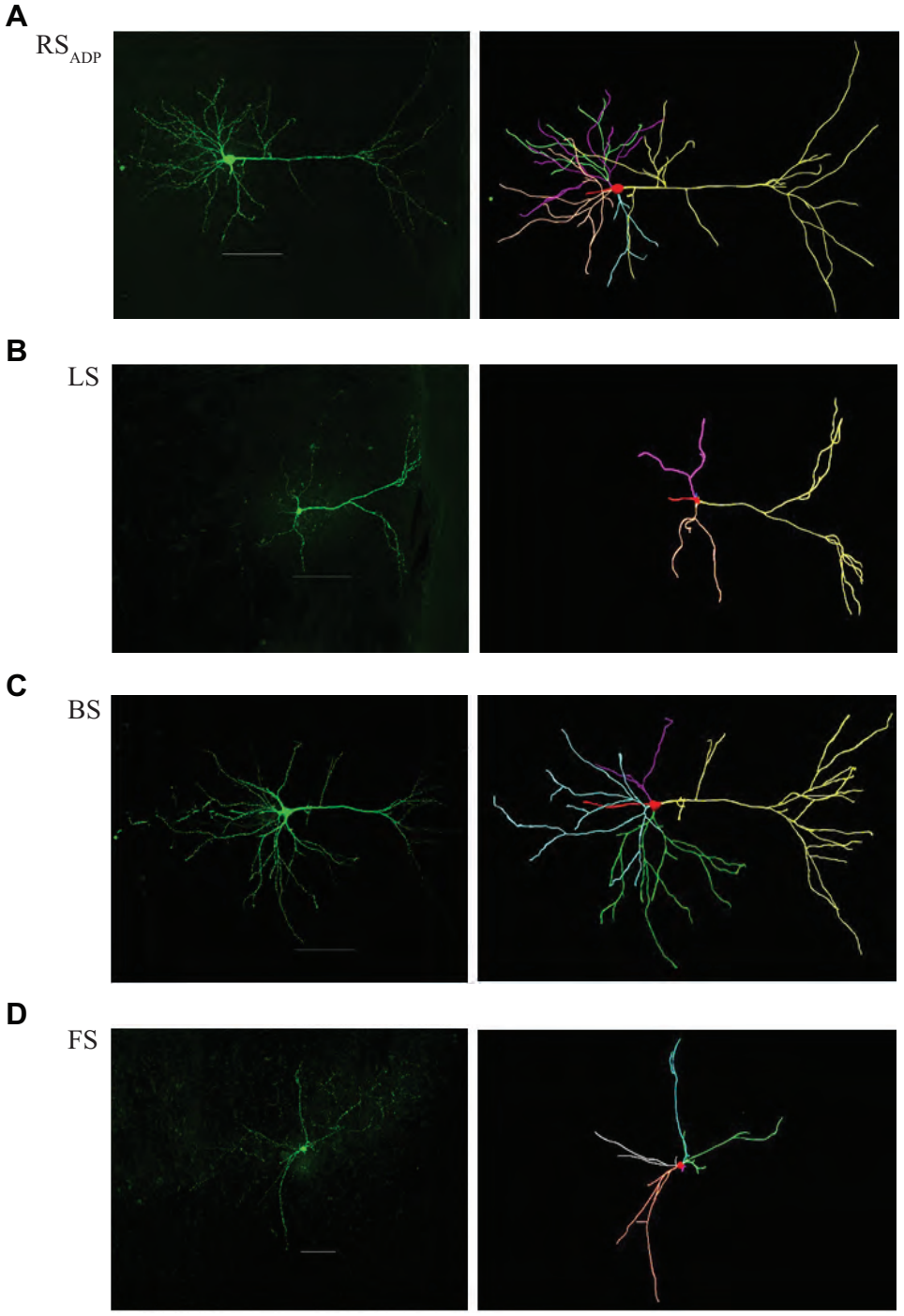

Fig. 6. Morphology of various classes of granular retrosplenial cortical (gRSC) neurons from adult rats. Shown are representative confocal *Z*-stack projections (*left*) and corresponding 3-dimensional reconstructions (*right*) of regular-spiking afterdepolarization (RS$_{ADP}$; *A*), late-spiking (LS; *B*), burst-spiking (BS; *C*), and fast-spiking (FS; *D*) neurons. Scale bar, 100 μm.

(73%, 52 of 71; Table 1). The resting membrane potential (RMP) of RS$_{ADP}$ neurons in L2/3 (-65.1 ± 1.4 mV; Table 2) was not different from L5 RS$_{ADP}$ neurons (-66.0 ± 0.5 mV; Table 2). However, R_N was significantly higher in L2/3 RS$_{ADP}$ neurons compared with L5 RS$_{ADP}$ neurons ($t_{69} = 2.839$, $P < 0.05$, independent *t*-test; Fig. 2*A*). In response to large hyperpolarizing currents, a sag in voltage responses was observed in both L2/3 and L5 RS$_{ADP}$ neurons; however, L5 RS$_{ADP}$ neurons had a significantly larger sag compared with L2/3 RS$_{ADP}$ neurons ($t_{67} = 2.1$, $P < 0.05$, independent *t*-test). Moreover, compared with all other firing types, L5 RS$_{ADP}$ neurons had a significantly higher sag [$F_{(4, 91)} = 5.4$, $P < 0.01$, 1-way ANOVA followed by Fisher's LSD post hoc test; Table 2]. In response to suprathreshold current injections, L2/3 RS$_{ADP}$ neurons had a decreased ISI and a higher initial firing frequency compared with L5 RS$_{ADP}$ neurons [$F_{(1, 69)} = 4.15$, $P < 0.05$, repeated-measures ANOVA; Fig. 2*B*]. RS$_{ADP}$ neurons in both layers demonstrated robust spike frequency adaptation (i.e., firing frequency rapidly decreased throughout the duration of the somatic current injection; see Fig. 2*B*).

Morphologically, L2/3 ($n = 5$) and L5 ($n = 38$) RS$_{ADP}$ neurons had similar somatic volumes ($t_{41} = 0.1$, $P > 0.05$, independent *t*-test; Fig. 7*A*) and surface areas ($t_{41} = 0.1$, $P > 0.05$, independent *t*-test; Fig. 7*B*). Furthermore, Sholl analysis

Table 1. *Developmental changes in neuronal firing type distribution*

	%RS	%RS_{ADP}	%LS	%BS	%FS
Adult (PND > 60)					
L2/3	2% (1)	38% (19)	58% (29)	0% (0)	2% (1)
L5	3% (2)	79% (52)	3% (2)	5% (3)	11% (7)
Juvenile (PND 14–30)					
L2/3	10% (1)	0% (0)	90% (9)	0% (0)	0% (0)
L5	81% (35)	12% (5)	0% (0)	5% (2)	2% (1)

Data indicate the percentage of each firing type observed as a function of layer (L2/3 or L5) and age (juvenile or adult). BS, burst spiking; FS, fast spiking; LS, late spiking; PND, postnatal day; RS, regular spiking; RS_{ADP}, regular spiking afterdepolarization; Nos. in parentheses are the no. of cells.

revealed no significant differences in dendritic branching between L2/3 and L5 RS_{ADP} neurons [$F_{(1, 41)} = 2.14$, $P > 0.05$, repeated-measures ANOVA, Fig. 7, *C* and *D*]. All 43 reconstructed RS_{ADP} neurons possessed numerous spines on their apical and basilar dendrites (data not shown).

Physiology and Morphology of LS Neurons in L2/3 of the Adult gRSC

LS neurons were predominantly found in L2/3 of the adult gRSC (93%, 29 of 31; Table 1) and were identified as pyramidal. They had minimal sag and showed little inward rectification current (Table 2 and Fig. 3*A*). One distinguishing membrane feature of LS neurons was their significantly higher R_N (489.3 ± 23.4 MΩ; Table 2) compared with all other firing types [$F_{(4, 109)} = 121.2$, $P < 0.001$, 1-way ANOVA followed Fisher's LSD post hoc test; Table 2]. In addition, they had a more hyperpolarized RMP compared with RS_{ADP} as well as FS neurons [$F_{(4, 109)} = 6.236$, $P < 0.001$, 1-way ANOVA followed Fisher's LSD post hoc test; Table 2]. Unlike any other firing type, LS neurons did not fire shortly after the onset of a depolarizing current injection. Rather, they had a significantly longer latency to first AP compared with all other gRSC cell types [$F_{(4, 109)} = 63.318$, $P < 0.001$, 1-way ANOVA followed Fisher's LSD post hoc test; Table 2 and Fig. 3]. $AP_{latency}$ shortened in response to increasing depolarizing currents, but there was still a distinctive delay as the membrane potential ramped upward before initiation of the first AP (see Fig. 3*B*). In contrast to RS_{ADP} and BS neurons that exhibited a rapid reduction in firing frequencies, LS neurons maintained high-firing frequencies throughout the somatic current injection (see Fig. 3*B*).

Overall, LS neurons in L2/3 ($n = 20$) had the highest R_N (Table 2) and the smallest somatic surface area compared with all other firing types [$F_{(4, 69)} = 4.142$, $P < 0.01$, 1-way ANOVA followed Fisher's LSD post hoc test; Fig. 7*B*]. Sholl analysis revealed that LS neurons had significantly fewer intersections and less dendritic branching compared with L2/3 RS_{ADP} neurons [$F_{(1, 23)} = 20.721$, $P < 0.001$, repeated-measures ANOVA; Fig. 7*C*]. Compared with RS_{ADP} and BS neurons, LS neurons appeared to have fewer spines on their apical and basilar dendrites (data not shown).

Physiology and Morphology of BS Neurons in L5 of the Adult gRSC

BS pyramidal neurons generated a burst of two or more APs in response to a suprathreshold-depolarizing current injection (Fig. 4*A*). No BS neurons were observed in L2/3, and ~5% (3 of 66; Table 1) of L5 gRSC neurons were identified as BS neurons, but unlike RS_{ADP} neurons, BS neurons do not have a depolarizing sag in response to large hyperpolarizing current injections (Table 2 and Fig. 4*A*). Similar to RS_{ADP} neurons, BS neurons are able to adapt in response to depolarizing current

Table 2. *Intrinsic membrane properties of the different classes of adult gRSC neurons*

	RS_{ADP}				
	L2/3 ($n = 19$)	L5 ($n = 52$)	LS (L2/3; $n = 29$)	BS (L5; $n = 3$)	FS (L5; $n = 7$)
Membrane Properties					
RMP, mV	−65.1 ± 1.4***	−66.0 ± 0.5***	−70.8 ± 1.0	−66.7 ± 2.7	−65.6 ± 1.9*
R_N, MΩ	140.1 ± 20.2***	99.3 ± 5.0***	489.3 ± 23.4	125.1 ± 47.4***	108.0 ± 12.8***
τ, ms	37.9 ± 1.7***#	39.5 ± 0.9***#	50.1 ± 0.8#	41.2 ± 5.5*#	31.6 ± 3.0***
Sag, %	0.2 ± 0.0	0.4 ± 0.1***#‡	0.1 ± 0.0	0.1 ± 0.0	0.1 ± 0.0
Post-burst AHP					
AHP_{peak}, mV	−3.3 ± 0.2#	−3.5 ± 0.1#	−3.8 ± 0.3#	−3.1 ± 1.0	−1.9 ± 0.3
AHP_{peak}, ms	88.4 ± 11.9*	80.4 ± 13.0**	163.4 ± 25.5	118.5 ± 38.5	117.2 ± 36.3
Rheobase properties					
$I_{threshold}$, pA	76.2 ± 9.7#	88.4 ± 8.2**#	50.0 ± 4.5#	67.3 ± 6.2#	139.3 ± 18.1**
$AP_{threshold}$, mV	−36.7 ± 0.8#	−37.2 ± 0.6#	−37.0 ± 0.7#	−34.7 ± 3.3#	−42.9 ± 2.2
$AP_{latency}$, ms	213.4 ± 29.2***	216.0 ± 11.8***	636.2 ± 34.0	210.4 ± 39.8***	110.1 ± 41.4***
$AP_{amplitude}$, mV	91.3 ± 2.7***	91.2 ± 1.0***	76.9 ± 2.0	91.3 ± 2.6*	86.8 ± 5.7*
fAHP, mV	14.4 ± 0.9*	14.0 ± 0.5**	19.7 ± 0.5	5.2 ± 0.0	12.1 ± 12.4*
mAHP, mV	20.2 ± 0.8#	20.1 ± 0.55#	19.7 ± 0.5#	22.8 ± 1.8#	13.6 ± 3.9
$AP_{half\text{-}width}$, μs	483.1 ± 21.2**#†	461.0 ± 9.2**#†	416.0 ± 11.5#†	637.3 ± 43.3***#	186.4 ± 32.1***†
$ADP_{amplitude}$, mV	3.2 ± 0.5*	3.5 ± 0.2**	4.8 ± 0.3	NA	NA

Values are means ± SE. $ADP_{amplitude}$, amplitude of the afterdepolarization following a single action potential; AHP, afterhyperpolarization; $AP_{amplitude}$, the amplitude of the first action potential; $AP_{half\text{-}width}$, duration of the action potential at half amplitude; $AP_{latency}$, latency to first action potential at rheobase; $AP_{threshold}$, membrane voltage at the start of an action potential; BS, burst spiking; fAHP, fast afterhyperpolarization; FS, fast spiking; $I_{threshold}$, current required to initiate an action potential; LS, late spiking; NA, not available; gRSC, granular retrosplenial cortical; mAHP, medium afterhyperpolarization; RMP, resting membrane potential; R_N, neuronal input resistance; RS_{ADP}, regular spiking afterdepolarization; Sag, depolarizing voltage response to a hyperpolarizing current injection; τ, membrane time constant. See METHODS for additional details on membrane properties. *$P < 0.05$, **$P < 0.01$,and ***$P < 0.001$,significantly different from LS neurons; #$P < 0.05$, significantly different from FS neurons; †$P < 0.05$, significantly different from BS neurons; ‡$P < 0.05$, significantly different between L2/3 and L5 RS_{ADP}.

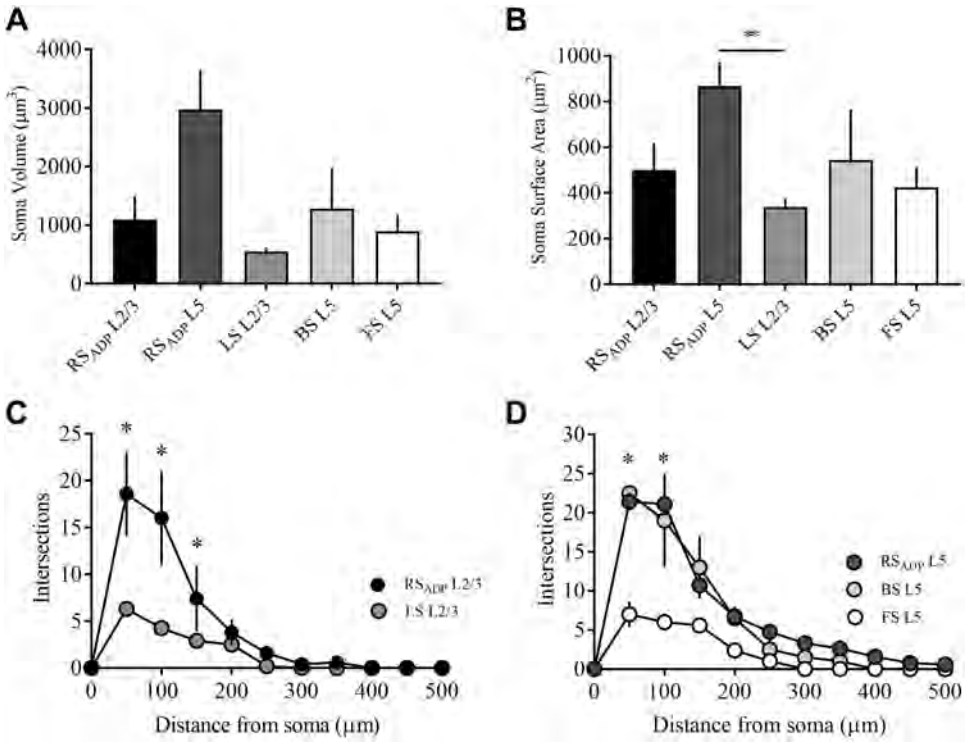

Fig. 7. Morphological properties of retrosplenial cortical (gRSC) neurons. *A*: plot of somatic volume as a function of cell type. One-way ANOVA revealed no significant group differences between the firing types ($P > 0.05$). *B*: plot of somatic surface area as a function of cell type. One-way ANOVA revealed a significant group effect of soma surface area ($P < 0.01$), and post hoc tests showed that L5 regular-spiking afterdepolarization (RS_{ADP}) neurons were significantly higher than L2/3 late-spiking (LS) neurons. *C*: Sholl analysis comparing dendritic branching of RS_{ADP} and LS neurons within L2/3 of adult gRSC. Repeated-measures ANOVA revealed that within L2/3, RS_{ADP} neurons have significantly more intersections and branching compared with LS neurons ($P < 0.01$). Post hoc tests showed that significant differences were observed at 50 μm, 100 μm, and 150 μm from the soma ($P < 0.05$). *D*: Sholl analysis comparing dendritic branching of cell types within L5 of adult gRSC. A repeated-measures ANOVA revealed that among L5 neurons, fast-spiking (FS) neurons are the most compact, having significantly fewer intersections and branching compared with RS_{ADP} and burst-spiking (BS) neurons ($P < 0.05$). Post hoc tests reveal that FS neurons have significantly fewer intersection at 50 μm and 100 μm from the soma (*$P < 0.05$; **$P < 0.01$).

injections (Fig. 4*B*). Morphologically, Sholl analysis revealed that BS neurons ($n = 2$) had dendritic branching most similar to L5 RS_{ADP} neurons [$F_{(1, 38)} = 28.288$, $P > 0.05$, repeated-measures ANOVA; Fig. 7*D*]. Spines were also observed on apical and basilar dendrites of BS neurons (data not shown).

Physiology and Morphology of FS Neurons in L5 of the Adult gRSC

FS neurons were primarily located in L5 (7 of 8; Table 1) and were identified as nonpyramidal at the time of the recordings. FS neurons in L5 had a similar R_N (108 ± 12.8 MΩ) to RS_{ADP} and BS neurons (Table 2). FS neurons had a minimal sag and showed no inward rectification current (Table 2 and Fig. 5*A*). FS neurons had a significantly reduced $AP_{threshold}$ [$F_{(4, 109)} = 62.886$, $P < 0.05$, 1-way ANOVA followed by Fisher's LSD post hoc test; Table 2], mAHP [$F_{(4, 109)} = 4.848$, $P < 0.01$, 1-way ANOVA followed by Fisher's LSD post hoc test; Table 2], and AHP peak amplitude [$F_{(4, 109)} = 3.384$, $P < 0.05$, 1-way ANOVA followed Fisher's LSD post hoc test; Table 2]. Initial firing frequencies of FS neurons were significantly higher compared with all other firing types [$F_{(4, 85)} = 15.298$, $P < 0.001$, repeated-measures ANOVA followed by Fisher's LSD post hoc test; Fig. 5*B*]. FS neurons fired repetitively and demonstrated little change in firing frequency throughout the somatic current injection (Fig. 5*B*). Although both FS and LS neurons demonstrated mild spike frequency adaptation, FS neurons have distinct spiking properties compared with LS neurons. For example, LS neurons have a uniquely higher R_N and longer $AP_{latency}$, which is not observed in FS neurons. Furthermore, FS neurons have a significantly reduced mAHP and post-burst AHP peak amplitude, which is not seen in LS neurons.

Morphologically, FS neurons ($n = 5$) in L5 had smaller somatic surface area (Fig. 7*B*) and significantly reduced dendritic branching compared with L5 RS_{ADP} [$F_{(2, 42)} = 4.934$, $P < 0.05$, repeated-measures ANOVA followed by Fisher's LSD post hoc test; Fig. 7*D*]. No spines could be visualized on the dendrites of FS neurons (data not shown).

Pharmacology Experiments

The ADP firing property in L2/3 and L5 of RS_{ADP} neurons was further examined by assessing whether blocking group 1 metabotropic glutamate receptors mGluR1 and mGluR5 would abolish the ADP in gRSC neurons, as had previously been reported elsewhere in the brain (Young et al. 2004). Once a neuron was identified as RS_{ADP}, 10 μM or 100 μM of LY367385 (mGluR1 antagonist) and MPEP (mGluR5 antagonist) were bath applied for 20 min. Bath application of LY367385 and MPEP significantly reduced the $ADP_{amplitude}$ at both concentrations [$F_{(2, 35)} = 30.61$, $P < 0.01$, 1-way ANOVA followed by Fisher's LSD post hoc test; Fig. 8], with no effect of dose ($P > 0.05$; Fig. 8).

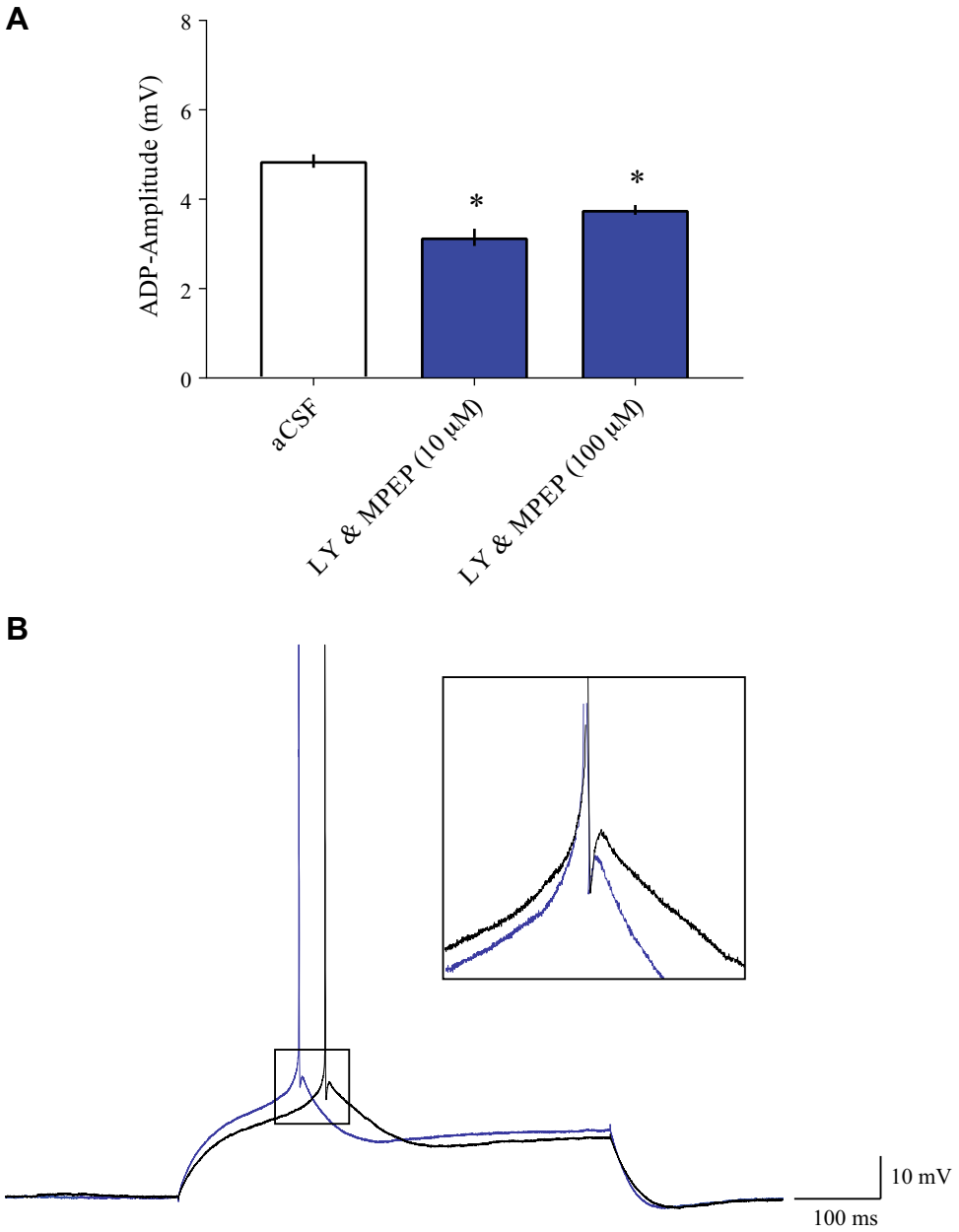

Fig. 8. Group 1 metabotropic glutamate receptors (mGluRs) partially mediate the ADP property in regular-spiking afterdepolarization (RS_{ADP}) neurons. *A*: plot of ADP amplitude before and after bath application of mGluR blockers. A 1-way ANOVA revealed a statistically significant main effect of aCSF on ADP amplitude [$F_{(2,\ 35)} = 30.61$, $P < 0.01$]. Post hoc analysis revealed that bath application of LY367385 and MPEP at both concentrations, 10 μM and 100 μM, significantly reduced ADP amplitude ($P < 0.01$ both comparisons), but the concentrations did not significantly differ in their effect ($P > 0.05$). *B*: overlay of membrane voltage responses before and after (traces in blue) bath application of mGluR blockers. Note the substantial effect of LY367385 and 2-methyl-6-(phenylethynyl) pyridine hydrochloride (MPEP) in reducing the ADP amplitude.

Postnatal Development of L5 gRSC Neurons

Similar to the findings of Kurotani et al. 2013, we observed that within L2/3 of the juvenile (PND 14–30) gRSC, 90% (9 of 10; Table 1) were LS neurons and only 10% were RS neurons. Within L5, RS neurons were the most common firing type (81%, 35 of 43; Table 1) in the juvenile gRSC, but this cell type was rare in L5 of the adult gRSC (3%, 2 of 66). In contrast, RS_{ADP} neurons were not common (12%, 5 of 43; Table 1) in L5 of the juvenile gRSC but were frequently observed (79%, 52 of 66; Table 1) in L5 of the adult gRSC. Interestingly, as illustrated in Fig. 9, intrinsic excitability was greater in the RS_{ADP} neurons in L5 of the adult gRSC compared with RS neurons in L5 of juvenile gRSC. This was evidenced by the fact that the adult neurons fired more APs in response to a series of depolarizing current injections. Differences in firing activity between juvenile and adult L5 gRSC neurons may be mediated by the slow afterhyperpolarization (sAHP), as juvenile gRSC neurons had a significantly larger sAHP (-2.03 ± 0.24 mV) compared with the slow AHP of adult RS_{ADP} neurons (-1.33 ± 0.18 mV; $t_{26} = 2.195$, $P < 0.05$, independent *t*-test).

DISCUSSION

Previous studies have exclusively used juvenile rats to study the intrinsic properties of neurons in the gRSC (Kurotani et al. 2013). Here, we demonstrate intrinsic and morphological characteristics of five distinct firing patterns, RS (L5), RS_{ADP} (L2/3 and L5), LS (L2/3), BS (L5), and FS (L5), in adult gRSC neurons. Moreover, the present study further examined the underlying mechanism of the prominent ADP property in RS_{ADP} neurons and found that it was partially mediated by mGluRs. Interestingly, in juvenile but not adult gRSC, we observed only RS neurons that had no ADP, suggesting that neuronal firing types in the gRSC change as a consequence of

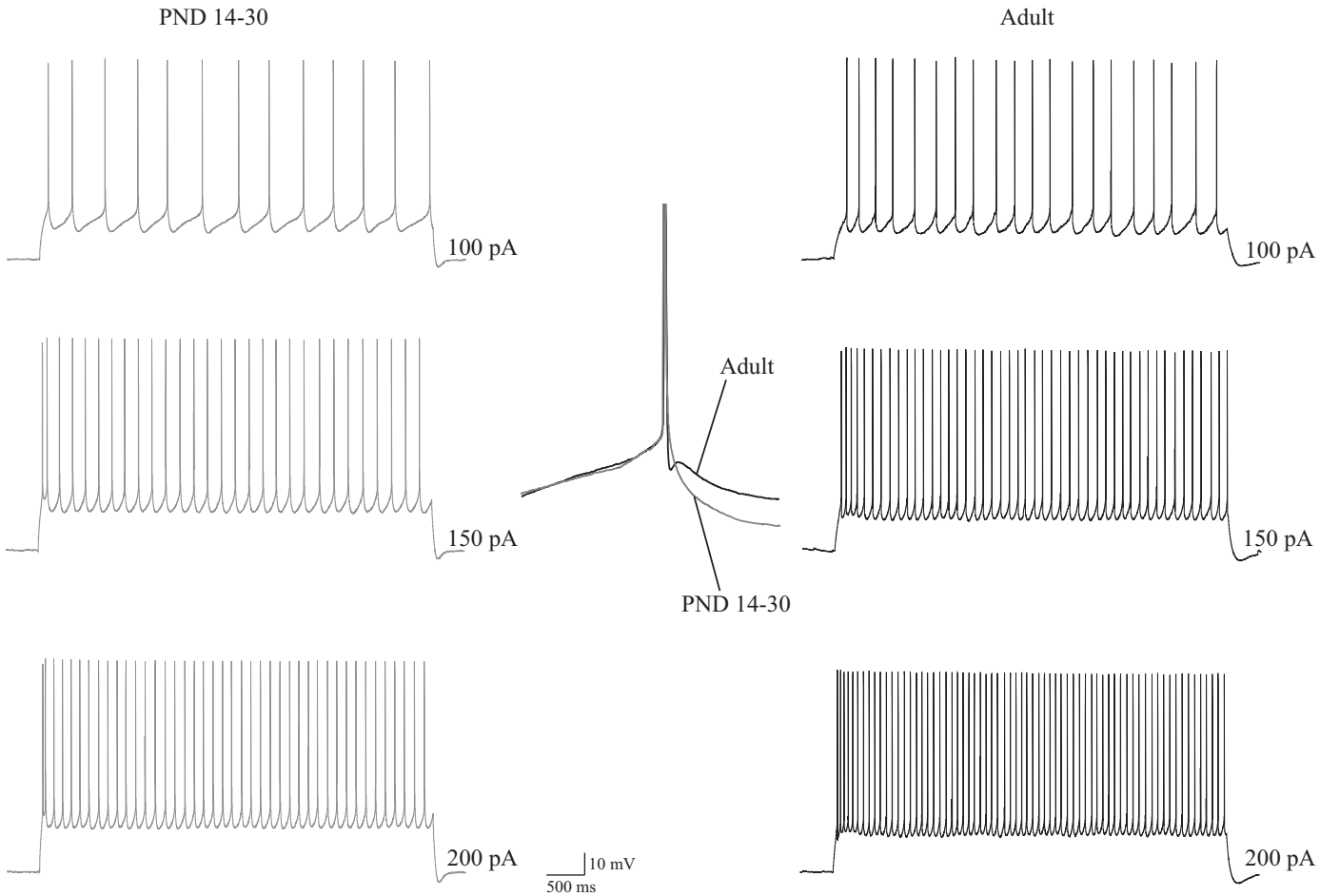

Fig. 9. Intrinsic plasticity within retrosplenial cortex (gRSC) during development. *Middle inset* shows an overlay of voltage responses illustrating that L5 neurons from juvenile rats [postnatal days (PND) 14–30] lack an afterdepolarization (ADP; gray sweeps), whereas L5 neurons from adult rats have a prominent ADP. *Left* and *right*: a series of membrane voltage responses to 5-s current injections. Regular-spiking (RS) neurons from juvenile rats (*left*) have reduced firing rates and a significantly larger slow afterhyperpolarization (sAHP; -2.03 ± 0.24 mV) compared with that of adult RS_{ADP} neurons (sAHP -1.33 ± 0.18 mV, $t_{26} = 2.195$, $P < 0.05$, independent *t*-test; *right*).

age and that emergence of the ADP may play a significant role in developmental changes in learning and memory.

Firing Types in Adult gRSC

RS_{ADP} neurons. RS_{ADP} neurons were observed in both L2/3 and L5; however, they were highly prevalent in L5 of the adult gRSC. Their morphological characteristics were similar, but they differed in certain intrinsic membrane properties. For example, RS_{ADP} neurons in L2/3 had a significantly higher initial firing frequency compared with those in L5. In addition to their presence in gRSC, RS_{ADP} neurons have also been observed in the CA1 (Azouz et al. 1996; Chen and Yaari 2008; Kaczorowski et al. 2007; Magee and Carruth 1999; Metz et al. 2005, 2007; Schwartzkroin 1975; Storm 1987; Yue and Yaari 2004; Yue et al. 2005) and CA3 (Brown and Randall 2009; Vervaeke et al. 2006) regions of the hippocampus, the prefrontal cortex (Haj-Dahmane and Andrade 1997, 1998; Kalmbach et al. 2013), and the lateral amygdala (Sugita et al. 1993). The ADP property following an AP can trigger burst firing in hippocampal neurons (Azouz et al. 1996; Jensen et al. 1996; Schwartzkroin 1975), and bursting is a requirement for synaptic plasticity at the Schaffer collateral to CA1 synapse (Pike et al. 1999; Thomas et al. 1998). Thus, the ADP shapes neuronal firing patterns and enhances excitability, which may play an important role in learning-related plasticity (Jensen et al. 1996; Moyer et al. 1996; Zhang and Linden 2003; Santini et al. 2008).

The ADP property following a single AP, or following a burst of APs, has been shown to be responsible for plastic changes and is mediated by *N*-methyl-D-aspartate receptors (Grienberger et al. 2014; Wu et al. 2004), mGluRs (Greene et al. 1994; Park et al. 2010; Young et al. 2004), and muscarinc receptors (Haj-Dahmane and Andrade 1998; Lei et al. 2014; Yan et al. 2009). For example, mGluR agonists induced an ADP and alter excitability in CA3 neurons of the hippocampus (Young et al. 2004). Moreover, activation of mGluRs and muscarinic receptors enhanced activity of Cav2.3 R-type Ca^{2+} channels in CA1 (Park et al. 2010), Ca^{2+}-activated nonselective cation (CAN) current in the neocortex (Greene et al. 1994), Na^{+} currents in the substantia nigra (Guatteo et al. 1999), and voltage-sensitive nonselective cation current in prefrontal cortex and CA3 of the hippocampus (Caeser et al. 1993; Haj-Dahmane and Andrade 1998). Our study sought to understand the mechanisms mediating the ADP in RS_{ADP} neurons of the gRSC. Although mGluR inhibitors (LY367385, mGluR1; and MPEP, mGluR5) significantly reduced the ADP in gRSC

neurons, they didn't completely abolish it (Fig. 8). Similarly, blockade of CAN currents with bath application of flufenamic acid (calcium-activated chloride channel blocker) reduced ADP amplitude but did not abolish it in the prefrontal cortex (Lei et al. 2014). A possible explanation for our results is that diverse receptors and channels contribute to the ADP and may differ across brain regions (Azouz et al. 1996; Chen and Yaari 2008; Fowler et al. 2007; Haj-Dahmane and Andrade 1997, 1998; Metz et al. 2005; Park et al. 2010; Yan et al. 2009). Future work is required to elucidate the precise mechanisms that mediate the ADP property in RS_{ADP} neurons of the gRSC.

BS neurons. In the gRSC, few BS neurons were observed in L5 that reliably fired in doublets or bursts (see Fig. 4). There were a subset of neurons that oscillated between single RS_{ADP} to BS neurons, and those neurons were not included in the data set. This oscillating pattern has previously been reported in neurons of the subthalamic nucleus, which may be facilitated by the activation of L-type Ca^{2+} currents, Ca^{2+}-activated inward currents, and Ca^{2+}-activated K^+ currents (Beurrier et al. 1999; Su et al. 2001). Moreover, previous evidence suggests that summation of ADPs can lead to burst or repetitive neuronal firing (Legendre and Poulain 1992; Kuehl-Kovarik et al. 2005; Su et al. 2001). BS neurons exhibit similar characteristics to RS_{ADP} neurons, and due to the large prevalence of ADPs in L5 of the gRSC, we speculate that BS neurons may be an extension of RS_{ADP} neurons. One possibility that is worth exploring is whether intrinsic plasticity is capable of converting an RS_{ADP} neuron to a BS neuron and whether such changes may occur during learning and/or across the lifespan.

LS neurons. Computational models demonstrate that LS neurons may play a role in encoding information over long time intervals and integrating synaptic input to form a contextual representation (McGann and Brown 2000; Tieu et al. 1999). LS neurons have been observed in a variety of brain structures including, the superior colliculus (Saito and Isa 2000), basolateral amygdala (Washburn and Moises 1992), CA1 of the hippocampus (Storm 1988), neostriatum (Nisenbaum et al. 1994; Nisenbaum and Wilson 1995), and frontal cortex (Kawaguchi 1995; Kawaguchi and Kubota 1997). Moreover, pyramidal LS neurons have been reported in high percentages in L2/3 (50%, Beggs et al. 2000), and L6 (90%, McGann et al. 2001) of the perirhinal cortex. LS neurons are a heterogenous firing type as their intrinsic or morphological properties may vary across brain regions. For example, LS neurons in L2/3 and L5 of perirhinal cortex, and basolateral amygdala, are predominantly pyramidal (Washburn and Moises 1992; Beggs et al. 2000; Moyer et al. 2002), whereas LS neurons in L6 of perirhinal cortex and frontal cortex have a non-pyramidal morphology (Kawaguchi 1995; McGann et al. 2001).

So far, one study has reported intrinsic and morphological properties of LS neurons in L2/3 of the gRSC in juvenile rats (PND 20–35) and found that LS neurons are pyramidal and most abundant in L2/3 of the gRSC (92%; see Kurotani et al. 2013). Our study examined LS neurons in L2/3 of the adult gRSC and found similar results. LS neurons in both juvenile and adult gRSC neurons had a high R_N and a small soma surface area and exhibited robust repetitive firing with mild spike frequency adaptation, characteristics similar to LS neurons of the rat perirhinal cortex (Beggs et al. 2000; McGann et al. 2001; Moyer et al. 2002). Moreover, the late-spiking property of LS neurons is mediated by delayed rectifier and A-type potassium channels (Kv1.1, Kv1.4, and Kv4.3; Kurotani et al. 2013). Thus, intrinsic and morphological properties of LS neurons in the gRSC do not undergo significant changes as a function of developmental age.

FS neurons. FS neurons were located in L5 and were the only nonpyramidal firing type observed in the gRSC. FS neurons are typically GABAergic interneurons, as observed in the frontal cortex and hippocampus (Freund and Buzsáki 1996; Kawaguchi 1995; Kawaguchi and Kubota 1997). Compared with other pyramidal neurons, FS neurons in the gRSC had reduced $AP_{half\text{-}width}$ and small soma size, which are characteristic of other cortical GABAergic interneurons (Karayannis et al. 2007; McCormick et al. 1985). Behaviorally, in vivo recordings have examined that FS neurons are differentially activated in the medial prefrontal cortex during a spatial radial arm maze (Insel and Barnes 2015). Activity of FS neurons was associated with movement and accompanied sensory stimulation, which suggests that FS neurons modulate influx of sensory information to the medial prefrontal cortex (Insel and Barnes 2015). Overall, the diversity of firing patterns in the gRSC indicates that the region is capable of dynamic information processing and higher-order associative learning (Faulkner and Brown 1999; Moyer et al. 2002).

Postnatal Development of gRSC Neurons

The current study establishes that RS_{ADP} neurons are the most ubiquitous pyramidal neurons found in L5 of the gRSC (~50%), the largest layer of the region. The ADP property is absent in juvenile gRSC neurons (PND 14–30), where the most common neuronal firing type is the RS neuron. Interestingly, in the present study, very few RS neurons were observed in adult gRSC neurons (only 2 of 66 L5 neurons). These data suggest that neuronal firing types in the gRSC are altered as a consequence of development, and the ADP property is a critical component that drives neuronal excitability and learning-related plasticity. Similar to the gRSC, neuronal physiology of the basolateral amygdala (BLA) undergoes significant changes as a function of age (Berdel and Moryś 2000; Brummelte et al. 2007; Dávila et al. 2008; Ehrlich et al. 2012; Moryś et al. 1998). Between PND 7–28, BLA neurons transitioned to a significantly reduced R_N, mAHP, fAHP, and hyperpolarized firing threshold (Ehrlich et al. 2012). Moreover, neurons in the BLA reached maturity on PND 28 (Ehrlich et al. 2012). Furthermore, in hippocampal pyramidal neurons, development of the hyperpolarization-activated excitatory current (I_h) and its underlying hyperpolarization-activated cyclic nucleotide-gated (HCN) channel, which are involved in shaping rhythmic firing and excitability, appeared around PND 20 (Vasilyev and Barish 2002). In parallel with neurophysiological changes, emergence of conditioned fear, including trace fear conditioning, did not appear until the first postnatal month in rats (Campbell and Ampuero 1985; Hunt et al. 1994; Kim and Richardson 2007; Moye and Rudy 1987; Sullivan et al. 2000). Taken together, the gRSC is a key node in the trace and context fear circuit; therefore, understanding the developmental trajectory of gRSC neurons is critical for therapeutic interventions for anxiety disorders.

Conclusion

In summary, the distinct morphologies and intrinsic properties of each firing type allow neurons to generate diverse firing patterns that may play a role in specific types of neuronal computations. Specifically, the ADP property in RS_{ADP} neurons has been shown to increase neuronal excitability and facilitate long-term potentiation (Azouz et al. 1996; Fortin and Bronzino 2001; Pike et al. 1999; Su et al. 2001; Thomas et al. 1998). This study elucidates the mechanisms underlying the ADP property of gRSC neurons, which may provide insight regarding the role of the gRSC in memory-related processes. Future investigations need to be conducted to understand how intrinsic properties of gRSC neurons may change as a function of learning and aging.

ACKNOWLEDGMENTS

We thank Chad W. Smies and Brendan R. Natwora for technical assistance and helpful feedback on the manuscript.

GRANTS

This study was supported by a Research Growth Initiative from the University of Wisconsin-Milwaukee (J.R.M.).

DISCLOSURES

No conflicts of interest, financial or otherwise, are declared by the authors.

AUTHOR CONTRIBUTIONS

H.Y., A.N.N., and J.R.M. conceived and designed research; H.Y. and A.N.N. performed experiments; H.Y. and A.N.N. analyzed data; H.Y., A.N.N., and J.R.M. interpreted results of experiments; H.Y. and A.N.N. prepared figures; H.Y. drafted manuscript; H.Y. and J.R.M. edited and revised manuscript; H.Y., A.N.N., and J.R.M. approved final version of manuscript.

REFERENCES

Albasser MM, Poirier GL, Warburton EC, Aggleton JP. Hippocampal lesions halve immediate-early gene protein counts in retrosplenial cortex: distal dysfunctions in a spatial memory system. *Eur J Neurosci* 26: 1254–1266, 2007. doi:10.1111/j.1460-9568.2007.05753.x.

Azouz R, Jensen MS, Yaari Y. Ionic basis of spike after-depolarization and burst generation in adult rat hippocampal CA1 pyramidal cells. *J Physiol* 492: 211–223, 1996. doi:10.1113/jphysiol.1996.sp021302.

Beggs JM, Moyer JR Jr, McGann JP, Brown TH. Prolonged synaptic integration in perirhinal cortical neurons. *J Neurophysiol* 83: 3294–3298, 2000. doi:10.1152/jn.2000.83.6.3294.

Berdel B, Moryś J. Expression of calbindin-D28k and parvalbumin during development of rat's basolateral amygdaloid complex. *Int J Dev Neurosci* 18: 501–513, 2000. doi:10.1016/S0736-5748(00)00024-1.

Beurrier C, Congar P, Bioulac B, Hammond C. Subthalamic nucleus neurons switch from single-spike activity to burst-firing mode. *J Neurosci* 19: 599–609, 1999. doi:10.1523/JNEUROSCI.19-02-00599.1999.

Brennan EKW, Sudhakar SK, Jedrasiak-Cape I, John TT, Ahmed OJ. Hyperexcitable Neurons Enable Precise and Persistent Information Encoding in the Superficial Retrosplenial Cortex. *Cell Reports* 30: 1598–1612.e8, 2020. doi:10.1016/j.celrep.2019.12.093.

Brown JT, Randall AD. Activity-dependent depression of the spike after-depolarization generates long-lasting intrinsic plasticity in hippocampal CA3 pyramidal neurons. *J Physiol* 587: 1265–1281, 2009. doi:10.1113/jphysiol.2008.167007.

Brummelte S, Witte V, Teuchert-Noodt G. Postnatal development of GABA and calbindin cells and fibers in the prefrontal cortex and basolateral amygdala of gerbils (Meriones unguiculatus). *Int J Dev Neurosci* 25: 191–200, 2007. doi:10.1016/j.ijdevneu.2007.01.002.

Caeser M, Brown DA, Gähwiler BH, Knöpfel T. Characterization of a calcium-dependent current generating a slow afterdepolarization of CA3 pyramidal cells in rat hippocampal slice cultures. *Eur J Neurosci* 5: 560–569, 1993. doi:10.1111/j.1460-9568.1993.tb00521.x.

Campbell BA, Ampuero MX. Dissociation of autonomic and behavioral components of conditioned fear during development in the rat. *Behav Neurosci* 99: 1089–1102, 1985. doi:10.1037/0735-7044.99.6.1089.

Chen LL, Lin L-H, Green EJ, Barnes CA, McNaughton BL. Head-direction cells in the rat posterior cortex. I. Anatomical distribution and behavioral modulation. *Exp Brain Res* 101: 8–23, 1994. doi:10.1007/BF00243212.

Chen S, Yaari Y. Spike Ca2+ influx upmodulates the spike afterdepolarization and bursting via intracellular inhibition of KV7/M channels. *J Physiol* 586: 1351–1363, 2008. doi:10.1113/jphysiol.2007.148171.

Cho J, Sharp PE. Head direction, place, and movement correlates for cells in the rat retrosplenial cortex. *Behav Neurosci* 115: 3–25, 2001. doi:10.1037/0735-7044.115.1.3.

Coelho CAO, Ferreira TL, Kramer-Soares JC, Sato JR, Oliveira MGM. Network supporting contextual fear learning after dorsal hippocampal damage has increased dependence on retrosplenial cortex. *PLOS Comput Biol* 14: e1006207, 2018. doi:10.1371/journal.pcbi.1006207.

Corcoran KA, Donnan MD, Tronson NC, Guzmán YF, Gao C, Jovasevic V, Guedea AL, Radulovic J. NMDA receptors in retrosplenial cortex are necessary for retrieval of recent and remote context fear memory. *J Neurosci* 31: 11655–11659, 2011. doi:10.1523/JNEUROSCI.2107-11.2011.

Corcoran KA, Frick BJ, Radulovic J, Kay LM. Analysis of coherent activity between retrosplenial cortex, hippocampus, thalamus, and anterior cingulate cortex during retrieval of recent and remote context fear memory. *Neurobiol Learn Mem* 127: 93–101, 2016. doi:10.1016/j.nlm.2015.11.019.

Cowansage KK, Shuman T, Dillingham BC, Chang A, Golshani P, Mayford M. Direct reactivation of a coherent neocortical memory of context. *Neuron* 84: 432–441, 2014. doi:10.1016/j.neuron.2014.09.022.

Dávila JC, Olmos L, Legaz I, Medina L, Guirado S, Real MÁ. Dynamic patterns of colocalization of calbindin, parvalbumin and GABA in subpopulations of mouse basolateral amygdalar cells during development. *J Chem Neuroanat* 35: 67–76, 2008. doi:10.1016/j.jchemneu.2007.06.003.

Ehrlich DE, Ryan SJ, Rainnie DG. Postnatal development of electrophysiological properties of principal neurons in the rat basolateral amygdala. *J Physiol* 590: 4819–4838, 2012. doi:10.1113/jphysiol.2012.237453.

Faulkner B, Brown TH. Morphology and physiology of neurons in the rat perirhinal-lateral amygdala area. *J Comp Neurol* 411: 613–642, 1999. doi:10.1002/(SICI)1096-9861(19990906)411:4<613:AID-CNE7>3.0.CO;2-U.

Fortin DA, Bronzino JD. The effect of interburst intervals on measures of hippocampal LTP in the freely moving adult male rat. *Exp Neurol* 170: 371–374, 2001. doi:10.1006/exnr.2001.7713.

Fowler MA, Sidiropoulou K, Ozkan ED, Phillips CW, Cooper DC. Corticolimbic expression of TRPC4 and TRPC5 channels in the rodent brain. *PLoS One* 2: e573, 2007. doi:10.1371/journal.pone.0000573.

Freund TF, Buzsáki G. Interneurons of the hippocampus. *Hippocampus* 6: 347–470, 1996. doi:10.1002/(SICI)1098-1063(1996)6:4<347:AID-HIPO1>3.0.CO;2-I.

Gabriel M, Lambert RW, Foster K, Orona E, Sparenborg S, Maiorca RR. Anterior thalamic lesions and neuronal activity in the cingulate and retrosplenial cortices during discriminative avoidance behavior in rabbits. *Behav Neurosci* 97: 675–696, 1983. doi:10.1037/0735-7044.97.5.675.

Garden DL, Massey PV, Caruana DA, Johnson B, Warburton EC, Aggleton JP, Bashir ZI. Anterior thalamic lesions stop synaptic plasticity in retrosplenial cortex slices: expanding the pathology of diencephalic amnesia. *Brain* 132: 1847–1857, 2009. doi:10.1093/brain/awp090.

Greene CC, Schwindt PC, Crill WE. Properties and ionic mechanisms of a metabotropic glutamate receptor-mediated slow afterdepolarization in neocortical neurons. *J Neurophysiol* 72: 693–704, 1994. doi:10.1152/jn.1994.72.2.693.

Grienberger C, Chen X, Konnerth A. NMDA receptor-dependent multidendrite Ca(2+) spikes required for hippocampal burst firing in vivo. *Neuron* 81: 1274–1281, 2014. doi:10.1016/j.neuron.2014.01.014.

Guatteo E, Mercuri NB, Bernardi G, Knöpfel T. Group I metabotropic glutamate receptors mediate an inward current in rat substantia nigra dopamine neurons that is independent from calcium mobilization. *J Neurophysiol* 82: 1974–1981, 1999. doi:10.1152/jn.1999.82.4.1974.

Haj-Dahmane S, Andrade R. Calcium-activated cation nonselective current contributes to the fast afterdepolarization in rat prefrontal cortex neurons. *J Neurophysiol* 78: 1983–1989, 1997. doi:10.1152/jn.1997.78.4.1983.

Haj-Dahmane S, Andrade R. Ionic mechanism of the slow afterdepolarization induced by muscarinic receptor activation in rat prefrontal cortex. *J Neurophysiol* 80: 1197–1210, 1998. doi:10.1152/jn.1998.80.3.1197.

Hunt PS, Richardson R, Campbell BA. Delayed development of fear-potentiated startle in rats. *Behav Neurosci* 108: 69–80, 1994. doi:10.1037/0735-7044.108.1.69.

Insel N, Barnes CA. Differential activation of fast-spiking and regular-firing neuron populations during movement and reward in the dorsal medial frontal cortex. *Cereb Cortex* 25: 2631–2647, 2015. doi:10.1093/cercor/bhu062.

Jensen MS, Azouz R, Yaari Y. Spike after-depolarization and burst generation in adult rat hippocampal CA1 pyramidal cells. *J Physiol* 492: 199–210, 1996. doi:10.1113/jphysiol.1996.sp021301.

Kaczorowski CC, Davis SJ, Moyer JR Jr. Aging redistributes medial prefrontal neuronal excitability and impedes extinction of trace fear conditioning. *Neurobiol Aging* 33: 1744–1757, 2012. doi:10.1016/j.neurobiolaging.2011.03.020.

Kaczorowski CC, Disterhoft J, Spruston N. Stability and plasticity of intrinsic membrane properties in hippocampal CA1 pyramidal neurons: effects of internal anions. *J Physiol* 578: 799–818, 2007. doi:10.1113/jphysiol.2006.124586.

Kalmbach BE, Chitwood RA, Dembrow NC, Johnston D. Dendritic generation of mGluR-mediated slow afterdepolarization in layer 5 neurons of prefrontal cortex. *J Neurosci* 33: 13518–13532, 2013. doi:10.1523/JNEUROSCI.2018-13.2013.

Karayannis T, Huerta-Ocampo I, Capogna M. GABAergic and pyramidal neurons of deep cortical layers directly receive and differently integrate callosal input. *Cereb Cortex* 17: 1213–1226, 2007. doi:10.1093/cercor/bhl035.

Kawaguchi Y. Physiological subgroups of nonpyramidal cells with specific morphological characteristics in layer II/III of rat frontal cortex. *J Neurosci* 15: 2638–2655, 1995. doi:10.1523/JNEUROSCI.15-04-02638.1995.

Kawaguchi Y, Kubota Y. GABAergic cell subtypes and their synaptic connections in rat frontal cortex. *Cereb Cortex* 7: 476–486, 1997. doi:10.1093/cercor/7.6.476.

Keene CS, Bucci DJ. Neurotoxic lesions of retrosplenial cortex disrupt signaled and unsignaled contextual fear conditioning. *Behav Neurosci* 122: 1070–1077, 2008a. doi:10.1037/a0012895.

Keene CS, Bucci DJ. Involvement of the retrosplenial cortex in processing multiple conditioned stimuli. *Behav Neurosci* 122: 651–658, 2008b. doi:10.1037/0735-7044.122.3.651.

Keene CS, Bucci DJ. Contributions of the retrosplenial and posterior parietal cortices to cue-specific and contextual fear conditioning. *Behav Neurosci* 122: 89–97, 2008c. doi:10.1037/0735-7044.122.1.89.

Keene CS, Bucci DJ. Damage to the retrosplenial cortex produces specific impairments in spatial working memory. *Neurobiol Learn Mem* 91: 408–414, 2009. doi:10.1016/j.nlm.2008.10.009.

Kim JH, Richardson R. A developmental dissociation in reinstatement of an extinguished fear response in rats. *Neurobiol Learn Mem* 88: 48–57, 2007. doi:10.1016/j.nlm.2007.03.004.

Kuehl-Kovarik MC, Partin KM, Handa RJ, Dudek FE. Spike-dependent depolarizing afterpotentials contribute to endogenous bursting in gonadotropin releasing hormone neurons. *Neuroscience* 134: 295–300, 2005. doi:10.1016/j.neuroscience.2005.03.047.

Kurotani T, Miyashita T, Wintzer M, Konishi T, Sakai K, Ichinohe N, Rockland KS. Pyramidal neurons in the superficial layers of rat retrosplenial cortex exhibit a late-spiking firing property. *Brain Struct Funct* 218: 239–254, 2013. doi:10.1007/s00429-012-0398-1.

Kwapis JL, Jarome TJ, Lee JL, Helmstetter FJ. The retrosplenial cortex is involved in the formation of memory for context and trace fear conditioning. *Neurobiol Learn Mem* 123: 110–116, 2015. doi:10.1016/j.nlm.2015.06.007.

Legendre P, Poulain DA. Intrinsic mechanisms involved in the electrophysiological properties of the vasopressin-releasing neurons of the hypothalamus. *Prog Neurobiol* 38: 1–17, 1992. doi:10.1016/0301-0082(92)90032-A.

Lei YT, Thuault SJ, Launay P, Margolskee RF, Kandel ER, Siegelbaum SA. Differential contribution of TRPM4 and TRPM5 nonselective cation channels to the slow afterdepolarization in mouse prefrontal cortex neurons. *Front Cell Neurosci* 8: 267, 2014. doi:10.3389/fncel.2014.00267.

Magee JC, Carruth M. Dendritic voltage-gated ion channels regulate the action potential firing mode of hippocampal CA1 pyramidal neurons. *J Neurophysiol* 82: 1895–1901, 1999. doi:10.1152/jn.1999.82.4.1895.

Martin SJ, Morris RG. New life in an old idea: the synaptic plasticity and memory hypothesis revisited. *Hippocampus* 12: 609–636, 2002. doi:10.1002/hipo.10107.

Maviel T, Durkin TP, Menzaghi F, Bontempi B. Sites of neocortical reorganization critical for remote spatial memory. *Science* 305: 96–99, 2004. doi:10.1126/science.1098180.

McCormick DA, Connors BW, Lighthall JW, Prince DA. Comparative electrophysiology of pyramidal and sparsely spiny stellate neurons of the neocortex. *J Neurophysiol* 54: 782–806, 1985. doi:10.1152/jn.1985.54.4.782.

McGann JP, Brown TH. Fear conditioning model predicts key temporal aspects of conditioned response production. *Psychobiology* 28: 303–313, 2000.

McGann JP, Moyer JR Jr, Brown TH. Predominance of late-spiking neurons in layer VI of rat perirhinal cortex. *J Neurosci* 21: 4969–4976, 2001. doi:10.1523/JNEUROSCI.21-14-04969.2001.

Metz AE, Jarsky T, Martina M, Spruston N. R-type calcium channels contribute to afterdepolarization and bursting in hippocampal CA1 pyramidal neurons. *J Neurosci* 25: 5763–5773, 2005. doi:10.1523/JNEUROSCI.0624-05.2005.

Metz AE, Spruston N, Martina M. Dendritic D-type potassium currents inhibit the spike afterdepolarization in rat hippocampal CA1 pyramidal neurons. *J Physiol* 581: 175–187, 2007. doi:10.1113/jphysiol.2006.127068.

Miller AM, Vedder LC, Law LM, Smith DM. Cues, context, and long-term memory: the role of the retrosplenial cortex in spatial cognition. *Front Hum Neurosci* 8: 586, 2014. doi:10.3389/fnhum.2014.00586.

Moryś J, Berdel B, Kowiański P, Dziewiatkowski J. The pattern of synaptophysin changes during the maturation of the amygdaloid body and hippocampal hilus in the rat. *Folia Neuropathol* 36: 15–23, 1998.

Moye TB, Rudy JW. Ontogenesis of trace conditioning in young rats: dissociation of associative and memory processes. *Dev Psychobiol* 20: 405–414, 1987. doi:10.1002/dev.420200405.

Moyer JR Jr, Brown TH. Methods for whole-cell recording from visually preselected neurons of perirhinal cortex in brain slices from young and aging rats. *J Neurosci Methods* 86: 35–54, 1998. doi:10.1016/S0165-0270(98)00143-5.

Moyer JR Jr, McNay EC, Brown TH. Three classes of pyramidal neurons in layer V of rat perirhinal cortex. *Hippocampus* 12: 218–234, 2002. doi:10.1002/hipo.1110.

Moyer JR Jr, Thompson LT, Disterhoft JF. Trace eyeblink conditioning increases CA1 excitability in a transient and learning-specific manner. *J Neurosci* 16: 5536–5546, 1996. doi:10.1523/JNEUROSCI.16-17-05536.1996.

Nisenbaum ES, Wilson CJ. Potassium currents responsible for inward and outward rectification in rat neostriatal spiny projection neurons. *J Neurosci* 15: 4449–4463, 1995. doi:10.1523/JNEUROSCI.15-06-04449.1995.

Nisenbaum ES, Xu ZC, Wilson CJ. Contribution of a slowly inactivating potassium current to the transition to firing of neostriatal spiny projection neurons. *J Neurophysiol* 71: 1174–1189, 1994. doi:10.1152/jn.1994.71.3.1174.

Park JY, Remy S, Varela J, Cooper DC, Chung S, Kang HW, Lee JH, Spruston N. A post-burst after depolarization is mediated by group i metabotropic glutamate receptor-dependent upregulation of Ca(v)2.3 R-type calcium channels in CA1 pyramidal neurons. *PLoS Biol* 8: e1000534, 2010. doi:10.1371/journal.pbio.1000534.

Pike FG, Meredith RM, Olding AW, Paulsen O. Rapid report: postsynaptic bursting is essential for 'Hebbian' induction of associative long-term potentiation at excitatory synapses in rat hippocampus. *J Physiol* 518: 571–576, 1999. doi:10.1111/j.1469-7793.1999.0571p.x.

Pothuizen HH, Davies M, Albasser MM, Aggleton JP, Vann SD. Granular and dysgranular retrosplenial cortices provide qualitatively different contributions to spatial working memory: evidence from immediate-early gene imaging in rats. *Eur J Neurosci* 30: 877–888, 2009. doi:10.1111/j.1460-9568.2009.06881.x.

Robinson S, Adelman JS, Mogul AS, Ihle PCJ, Davino GM. Putting fear in context: Elucidating the role of the retrosplenial cortex in context discrimination in rats. *Neurobiol Learn Mem* 148: 50–59, 2018. doi:10.1016/j.nlm.2017.12.009.

Robinson S, Poorman CE, Marder TJ, Bucci DJ. Identification of functional circuitry between retrosplenial and postrhinal cortices during fear conditioning. *J Neurosci* 32: 12076–12086, 2012. doi:10.1523/JNEUROSCI.2814-12.2012.

Saito Y, Isa T. Voltage-gated transient outward currents in neurons with different firing patterns in rat superior colliculus. *J Physiol* 528: 91–105, 2000. doi:10.1111/j.1469-7793.2000.00091.x.

Santini E, Quirk GJ, Porter JT. Fear conditioning and extinction differentially modify the intrinsic excitability of infralimbic neurons. *J Neurosci* 28: 4028–4036, 2008. doi:10.1523/JNEUROSCI.2623-07.2008.

Schwartzkroin PA. Characteristics of CA1 neurons recorded intracellularly in the hippocampal in vitro slice preparation. *Brain Res* 85: 423–436, 1975. doi:10.1016/0006-8993(75)90817-3.

Song C, Ehlers VL, Moyer JR Jr. Trace fear conditioning differentially modulates intrinsic excitability of medial prefrontal cortex-basolateral complex of amygdala projection neurons in infralimbic and prelimbic cortices. *J Neurosci* 35: 13511–13524, 2015. doi:10.1523/JNEUROSCI.2329-15.2015.

Song C, Moyer JR Jr. Layer- and subregion-specific differences in the neurophysiological properties of rat medial prefrontal cortex pyramidal neurons. *J Neurophysiol* 119: 177–191, 2018. doi:10.1152/jn.00146.2017.

Storm JF. Action potential repolarization and a fast after-hyperpolarization in rat hippocampal pyramidal cells. *J Physiol* 385: 733–759, 1987. doi:10.1113/jphysiol.1987.sp016517.

Storm JF. Temporal integration by a slowly inactivating K^+ current in hippocampal neurons. *Nature* 336: 379–381, 1988. [Erratum in *Nature* 336: 698: 1988.] doi:10.1038/336379a0.

Su H, Alroy G, Kirson ED, Yaari Y. Extracellular calcium modulates persistent sodium current-dependent burst-firing in hippocampal pyramidal neurons. *J Neurosci* 21: 4173–4182, 2001. doi:10.1523/JNEUROSCI.21-12-04173.2001.

Sugita S, Tanaka E, North RA. Membrane properties and synaptic potentials of three types of neurone in rat lateral amygdala. *J Physiol* 460: 705–718, 1993. doi:10.1113/jphysiol.1993.sp019495.

Sullivan RM, Landers M, Yeaman B, Wilson DA. Good memories of bad events in infancy. *Nature* 407: 38–39, 2000. doi:10.1038/35024156.

Tanaka KZ, Pevzner A, Hamidi AB, Nakazawa Y, Graham J, Wiltgen BJ. Cortical representations are reinstated by the hippocampus during memory retrieval. *Neuron* 84: 347–354, 2014. doi:10.1016/j.neuron.2014.09.037.

Thomas MJ, Watabe AM, Moody TD, Makhinson M, O'Dell TJ. Postsynaptic complex spike bursting enables the induction of LTP by theta frequency synaptic stimulation. *J Neurosci* 18: 7118–7126, 1998. doi:10.1523/JNEUROSCI.18-18-07118.1998.

Tieu K, Keidel A, McGann J, Faulkner B, Brown T. Perirhinal-amygdala circuit-level computational model of temporal encoding in fear conditioning. *Psychobiology* 27: 1–25, 1999. doi:10.3758/BF03332095.

Todd TP, Bucci DJ. Retrosplenial cortex and long-term memory: molecules to behavior. *Neural Plast* 2015: 1–9, 2015. doi:10.1155/2015/414173.

van Groen T, Kadish I, Wyss JM. Retrosplenial cortex lesions of area Rgb (but not of area Rga) impair spatial learning and memory in the rat. *Behav Brain Res* 154: 483–491, 2004. doi:10.1016/j.bbr.2004.03.016.

van Groen T, Vogt BA, Wyss JM. Interconnections between the thalamus and retrosplenial cortex in the rodent brain. In: *Neurobiology of Cingulate Cortex and Limbic Thalamus*, edited by Vogt BA and Gabriel M. New York: Springer, 1993, p. 123–150.

van Groen T, Wyss JM. Connections of the retrosplenial granular a cortex in the rat. *J Comp Neurol* 300: 593–606, 1990. doi:10.1002/cne.903000412.

Vasilyev DV, Barish ME. Postnatal development of the hyperpolarization-activated excitatory current Ih in mouse hippocampal pyramidal neurons. *J Neurosci* 22: 8992–9004, 2002. doi:10.1523/JNEUROSCI.22-20-08992.2002.

Vervaeke K, Gu N, Agdestein C, Hu H, Storm JF. Kv7/KCNQ/M-channels in rat glutamatergic hippocampal axons and their role in regulation of excitability and transmitter release. *J Physiol* 576: 235–256, 2006. doi:10.1113/jphysiol.2006.111336.

Washburn MS, Moises HC. Electrophysiological and morphological properties of rat basolateral amygdaloid neurons in vitro. *J Neurosci* 12: 4066–4079, 1992. doi:10.1523/JNEUROSCI.12-10-04066.1992.

Wu WW, Chan CS, Disterhoft JF. Slow afterhyperpolarization governs the development of NMDA receptor-dependent afterdepolarization in CA1 pyramidal neurons during synaptic stimulation. *J Neurophysiol* 92: 2346–2356, 2004. doi:10.1152/jn.00977.2003.

Yamawaki N, Corcoran KA, Guedea AL, Shepherd GM, Radulovic J. Differential contributions of glutamatergic hippocampal→retrosplenial cortical projections to the formation and persistence of context memories. *Cereb Cortex* 29: 2728–2736, 2019. doi:10.1093/cercor/bhy142.

Yan HD, Villalobos C, Andrade R. TRPC Channels Mediate a Muscarinic Receptor-Induced Afterdepolarization in Cerebral Cortex. *J Neurosci* 29: 10038–10046, 2009. doi:10.1523/JNEUROSCI.1042-09.2009.

Young SR, Chuang SC, Wong RK. Modulation of afterpotentials and firing pattern in guinea pig CA3 neurones by group I metabotropic glutamate receptors. *J Physiol* 554: 371–385, 2004. doi:10.1113/jphysiol.2003.051847.

Yue C, Remy S, Su H, Beck H, Yaari Y. Proximal persistent Na^+ channels drive spike afterdepolarizations and associated bursting in adult CA1 pyramidal cells. *J Neurosci* 25: 9704–9720, 2005. doi:10.1523/JNEUROSCI.1621-05.2005.

Yue C, Yaari Y. KCNQ/M channels control spike afterdepolarization and burst generation in hippocampal neurons. *J Neurosci* 24: 4614–4624, 2004. doi:10.1523/JNEUROSCI.0765-04.2004.

Zhang W, Linden DJ. The other side of the engram: experience-driven changes in neuronal intrinsic excitability. *Nat Rev Neurosci* 4: 885–900, 2003. doi:10.1038/nrn1248.